ELSEVIER

OVERVIEW OF IMAGE-GUIDED RADIATION THERAPY

Lei Xing, Ph.D., Brian Thorndyke, Ph.D., Eduard Schreibmann, Ph.D.,
Yong Yang, Ph.D., Tian-Fang Li, Ph.D., Gwe-Ya Kim, Ph.D., Gary Luxton, Ph.D.,
and Albert Koong, M.D.

Department of Radiation Oncology, Stanford University School of Medicine, Stanford, CA

Abstract—Radiation therapy has gone through a series of revolutions in the last few decades and it is now possible to produce highly conformal radiation dose distribution by using techniques such as intensity-modulated radiation therapy (IMRT). The improved dose conformity and steep dose gradients have necessitated enhanced patient localization and beam targeting techniques for radiotherapy treatments. Components affecting the reproducibility of target position during and between subsequent fractions of radiation therapy include the displacement of internal organs between fractions and internal organ motion within a fraction. Image-guided radiation therapy (IGRT) uses advanced imaging technology to better define the tumor target and is the key to reducing and ultimately eliminating the uncertainties. The purpose of this article is to summarize recent advancements in IGRT and discussed various practical issues related to the implementation of the new imaging techniques available to radiation oncology community. We introduce various new IGRT concepts and approaches, and hope to provide the reader with a comprehensive understanding of the emerging clinical IGRT technologies. Some important research topics will also be addressed.   © 2006 American Association of Medical Dosimetrists.

Key Words: IGRT, Organ motion, Image guidance, Dose optimization, 4D imaging.

INTRODUCTION

Radiotherapy is an image-guided intervention, and imaging is involved in every key step of the process, ranging from patient staging, simulation, treatment planning, and radiation delivery, to patient follow-up. The evolution of radiation therapy has been strongly correlated with the development of imaging techniques. During the early days when Roentgen first discovered x-rays, 2-dimensional (2D) transmission images of the human body provided unprecedented imagery of bony landmarks, which allowed radiologists to deduce the location of internal organs. Using planar radiographs, radiologists planned cancer treatments by collimating rectangular fields that circumscribed the presumed tumor location. Additional blocks placed daily to match marks on the patient's skin, and later using low-temperature-melting dense alloys. The emergence of computed tomography (CT) in the 1970s revolutionized radiation therapy and allowed us to use image data to build a 3-dimensional (3D) patient model and design 3D conformal radiation treatment. In general, 3D conformal radiation therapy (3DCRT) is a method of irradiating a tumor target volume defined in a 3D anatomical image of the patient with a set of x-ray beams individually shaped to conform to the 2D beam's-eye-view (BEV) projection of the target. The reduction in normal tissue irradiation when moving

from 2D to 3D should theoretically improve the therapeutic ratio and allow the tumor target volume to be treated to a higher dose, thereby improving the probability of tumor control. Recent technical advances in planning and delivering intensity-modulated radiation therapy (IMRT) provide an unprecedented means for producing exquisitely shaped radiation doses that closely conform to the tumor dimensions while sparing sensitive structures.[1–3] The development of 3DCRT and IMRT places more stringent requirements on the accuracy of beam targeting. In practice, large uncertainties exist in tumor volume delineation and in target localization due to intra- and inter-organ motions. The utility of modern radiation technologies, such as 3DCRT and IMRT, cannot be fully exploited without eliminating or significantly reducing these uncertainties. The need to improve targeting in radiation treatment has recently spurred a flood of research activities in image-guided radiation therapy (IGRT).

While all radiation therapy procedures are image guided *per se*, traditionally, imaging technology has primarily been used in producing 3D scans of the patient's anatomy to identify the location of the tumor prior to treatment. The verification of a treatment plan is typically done at the level of beam portals relative to the patient's bony anatomy before patient treatment. In current literature, the term of IGRT or IG-IMRT is employed loosely to refer to newly emerging radiation planning, patient setup, and delivery procedures that integrate cutting-edge image-based tumor definition methods, pa-

tient positioning devices, and/or radiation delivery guiding tools. These techniques combine new imaging tools, which interface with the radiation delivery system through hardware or software, and state-of-the-art 3DCRT or IMRT, and allow physicians to optimize the accuracy and precision of the radiotherapy by adjusting the radiation beam based on the true position of the target tumor and critical organs. With IGRT, it is also possible to take tumor motion into account during radiation therapy planning and treatment. Because IGRT improves precision, it raises the possibility of shortening the duration of radiation therapy by reducing the number of treatment sessions for some forms of cancer.

The purpose of this article is to highlight the recent developments of various available imaging techniques and present an overview of IGRT. Stanford experience on various aspects of clinical IGRT will also be presented. We hope that readers will gain an overall picture of IGRT and find it easier to navigate themselves through the subsequent articles in this issue, which focus on providing technical details and/or specific clinical applications of the available IGRT tools.

ISSUES IN IGRT

In current 3DCRT or IMRT, uncertainties exist in many circumstances, such as tumor target definition, patient immobilization, and patient breathing motion, which make it difficult to administer a high radiation dose to the planned location. The exact locations of the boundaries of the tumor target and the adjacent sensitive structures are often not known precisely, and a population- and disease site-based safety margin is used routinely to cope with a problem that is otherwise insoluble. An important task of IGRT is to eliminate or significantly reduce the margins involved in defining the clinical and planning target volume (CTV and PTV, respectively).

Many IGRT solutions have been proposed to resolve the problem of target definition and beam targeting. Briefly, IGRT developments are focused in four major areas: (1) biological imaging tools for better definition of tumor volume; (2) time-resolved (4D) imaging techniques for modeling the intra-fraction organ motion; (3) on-board imaging system or imaging devices registered to the treatment machines for inter-fraction patient localization; and (4) new radiation treatment planning and delivery schemes incorporating the information derived from the new imaging techniques. These are discussed in more detail in the following.

TUMOR TARGET VOLUME DEFINITION

CT, MRI, and ultrasound (US) imaging techniques

To be able to "see" the extent of disease more clearly and define the tumor target volume relative to the patient's anatomy have been among the most important issues in radiation oncology. CT has played a pivotal role in the process. Many radiation oncology departments have acquired dedicated CT scanners. A typical patient's 3D CT data set has more than 100 axial slices, each of which contains 512×512 pixels. With 16 bits per pixel, a CT data set can easily run over 50 megabytes. CT has many advantages, including high spatial integrity, high spatial resolution, excellent bony structure depiction, and the ability to provide relative electron density information used for radiation dose calculation. The recent development of ultra-fast multi-slice CT has opened a new dimension to CT technology and allows time-resolved (4D) CT imaging of patient's cardiac and breathing cycles. Using array detectors, multisection CT scanners can acquire multiple slices or sections simultaneously and thereby greatly increase the speed of CT image acquisition. Currently, all manufactures are moving toward 8-, 16- and even higher slice CT technology. Radiation oncology application of 4D CT will be discussed later.

MRI provides superior soft tissue discrimination, especially for central nervous system (CNS) structures and within the abdomen and pelvis, and has been widely used in the diagnosis and tumor delineation. MRI is also utilized for virtual simulation of radiation treatment for some specific disease sites. Physically, MRI involves the determination of the bulk magnetization of nuclei within a given voxel through use of radio-frequency (RF) radiation and magnetic fields. In a clinical setting, MRI is typically employed together with CT images with the help of image fusion software to delineate the extent of the malignancy. As with other imaging techniques, MR technology has gone through a series of revolutions in the past 3 decades. MRI technology is moving toward higher field strengths to further improve the quality of MR images, as evidenced by the installations of 3T scanners in many institutions (9.4 T MRI scanners have been installed in a few institutions). Fast-cine MRI is also becoming increasingly available and may offer physicians an alternative for imaging the temporal process of patient breathing or even heart beating. Figure 1 shows an example of MRI images acquired at 2 different phases for a liver cancer patient. In addition, the development of some specialized MRI scans has also attracted much attention. These include diffusion and perfusion MRI, dynamic contrast MRI, MR angiography, MR spectroscopic imaging (MRSI), and functional MRI (fMRI). The recent development of diffusion tensor imaging (DTI), for instance, enables diffusion to be measured in multiple directions and the fractional anisotropy in each direction to be calculated for each voxel. fMRI measures signal changes in the brain that are due to changing neural activity. These techniques enable researchers to make axonal and functional maps to examine the structural connectivity of different regions in the brain and may allow better definition of brain tumors and better sparing of sensitive regions.[4]

Ultrasound (US) is another useful imaging modality for radiation therapy. US utilizes high-frequency ($1{\sim}10$
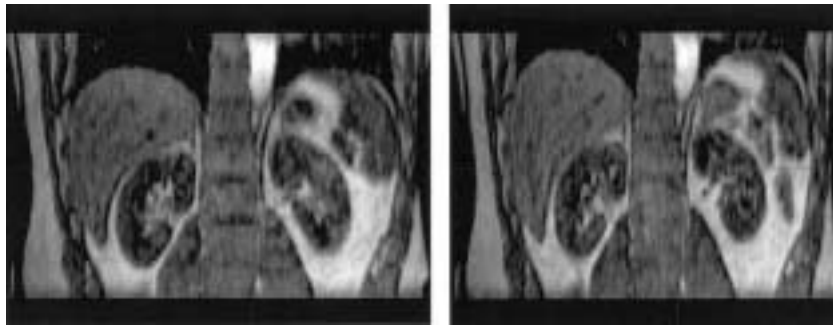
Fig. 1. Cine MR images at inhale and exhale phases for a liver cancer patient.

MHz) sound waves to generate anatomical images that have high spatial resolution and tissue characterization discrimination power through image texture analysis. In radiation therapy, it has been particularly useful in prostate imaging. Transrectal US permits an examination/localization of the prostate gland[5,6] and is the imaging modality of choice in guiding the prostate seed implant procedure.

Biological imaging

Regardless of the course of therapy, current standard imaging modalities such as CT and MRI do not always provide an accurate picture of the tumor extent, especially in the zone of infiltration that may be the limiting factor in an attempt of a radical treatment approach. This has been shown to be the case for gliomas before surgical intervention. It is also true when attempting to determine the volume of residual tumor for additional therapy owing to problems in differentiating post-therapy changes from residual tumor. Indeed, the above-mentioned imaging modalities are anatomic in nature, *i.e.*, they provide snapshot of a patient's anatomy without biological information of various organs or structures. Biological imaging, defined as the *in vivo* characterization and measurement of biological processes at the cellular and molecular level, is an emerging multidisciplinary field resulting from the developments of molecular biology and diagnostic imaging and shows significant promise to revolutionize cancer detection, staging/re-staging, treatment decision-making, and assessment of therapeutic response. MRSI and positron emission tomography (PET) are 2 valuable modalities for radiation therapy planning. ^{1}H MRSI combines the advantages of obtaining biochemical data by water-suppressed ^{1}H MR spectroscopy with the spatial localization of that data. MR spectroscopy is useful in characterization of brain and prostate tumors. In the brain, for example, malignant tumors have an increased rate of membrane turnover (increased level of choline) and a decreased concentration of neurons. Furthermore, spectroscopy allows for the noninvasive monitoring of the response of residual tumor to therapy and for differentiating tumor recurrence

from tissue necrosis. Recently, Pirzkall *et al.*[7] have applied multi-voxel MRSI to assess the impact of MRSI on the target volumes used for radiation therapy treatment planning for high-grade gliomas. It was found that, although T_2-weighted MRI estimated the region at risk of microscopic disease as being as much as 50% greater than by MRSI, metabolically active tumor tissue still extended outside the T_2 region in 88% of patients by as much as 28 mm. In addition, T_1-weighted MRI suggested a lesser volume and different location of active disease compared to MRSI. The discordance of high-grade-glioma target volumes resulting from MRI was also observed in other functional imaging modalities such as (PET) and single-photon emission computed tomography (SPECT).

While there is a growing body of evidence now indicating that *in vivo* MRSI provides unique information on metabolism that will ultimately affect clinical diagnosis, choice and monitoring of therapies, and treatment planning, in reality, MRSI has mainly remained a research tool confined to a small number of academic institutions.[8–12] PET, on the other hand, is more widely used and has been harnessed into the planning process in many clinics. In general, PET has lower image resolutions than CT images and, with commonly used fluorine-18-labeled deoxyglucose (FDG) tracer, contains no anatomic information about normal structures. Information derived from PET needs to be fused with the corresponding CT images for treatment planning. The fusion of PET and CT images are simplified with the use of the hybrid PET/CT scanner.[13,14] Figure 2 shows the data flow of a typical PET/CT scanner.

Hybrid PET/CT systems have several positive features that are absent in stand-alone PET and CT units. PET/CT is a hardware-based image-fusion technology that virtually eliminates the uncertainty and inconvenience of currently available software fusion of separate PET and CT images, which are often acquired with patients in different positions. It should be emphasized that the PET/CT unit is not simply a PET and CT combination—not from the perspective of system design, nor the practical utility. Other than the fact that one does
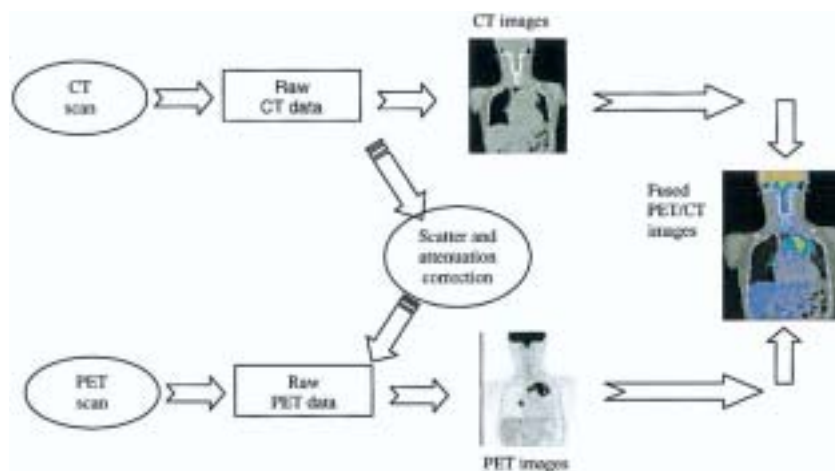
Fig. 2. Schematic drawing of the data flow in a hybrid PET/CT.

not have to go through the cumbersome and time consuming software fusion process, it has the advantages of simultaneous availability of the fused images, convenience to the patient and the physician, increased physician confidence in interpreting the image findings, and ~30% of reduction in PET scanning time due to the use of CT data for PET attenuation correction.

Integration of biological imaging techniques and multimodality image fusion

FDG-PET provides a means to study metabolic activity of tumors *in vivo*. Initial studies incorporating FDG-PET into treatment planning have been reported.[15–17] Bradley *et al*.[17] have carried out a prospective study to determine the impact of functional imaging with FDG-PET on target volumes among non-small cell lung cancer (NSCLC) patients being considered for definitive radiation therapy. They found that radiation targeting with fused FDG-PET and CT images resulted in alterations in radiation therapy planning in over 50% of patients by comparison with CT targeting. The changes included the alterations in the AJCC TNM stage (31% of the patients studied) and modification of target volume (58% of the patients studied). In a separate study, Mac-Manus *et al*.[16] reported that 30% of patients with locally-advanced NSCLC became ineligible for curative radiotherapy because of detection of either distant metastatic disease or intrathoracic disease too extensive for radical radiation. Recently, Howard *et al*.[18] have studied the value of FDG-PET/CT for esophagus cancer and reported similar findings.

Emerging PET tracers for oncologic imaging

While FDG-PET has been shown to be effective for a number of malignancies, imaging of many other neoplasms, such as breast cancer and prostate cancer, with FDG has shown less success.[19,20] Many pitfalls have previously been described with FDG-PET imaging. The FDG tracer can be nonspecifically taken up by several benign conditions such as inflammatory disease, pneumonia, brown fat, muscle, bowel uptake, and granulomatous disease. Also, slow-growing indolent tumors may exhibit only a mild increase in glucose metabolism and therefore be missed by FDG-PET.[21–23] Thus, FDG-PET is only minimally useful for the evaluation of indolent tumors such as organ-confined prostate cancer. The recent development of fluorothymidine (FLT)[24–26] provided a new opportunity to improve the sensitivity and specificity of PET imaging of cancer. Because there is upregulation of thymidine transport into malignant cells due to accelerated deoxyribonucleic acid synthesis, either ^{11}C or ^{18}F-labeled thymidine radiotracers can be used to determine cellular proliferation. Several studies have shown that the accumulation of FLT correlates better with proliferation in comparison with the commonly used FDG tracer.[25,26] Recently, Smyczek-Gargya *et al*.[27] have reported FLT-PET imaging experiments involving 12 patients with 14 primary breast cancer lesions (T2–T4). Thirteen of the 14 primary tumors demonstrated focally increased FLT uptake. The study showed that FLT-PET is suitable for the diagnosis of primary breast cancer and locoregional metastases and the high image contrast of the technique may facilitate the detection of small foci.

Agents, such as antisense molecules, aptamers, antibodies, and antibody fragments, can be aimed at molecular targets for biological imaging. Tumor receptors and certain cellular physiologic activities, including metabolism, hypoxia, proliferation, apoptosis, angiogenesis, and infection, provide such targets. In addition to FLT, there are several other new nuclide imaging tracers under clinical or laboratory investigations,[21,28–35] which include, to name a few, ^{11}C-Acetate,[36–38] ^{18}F-choline,[39,40] ^{11}C-choline,[41,42] ^{64}Cu-DOTA-Bombesin,[43] ^{18}F-FMISO,[44,45] ^{18}F-FAZA,[46] ^{64}Cu-ATSM.[47] For example, carcinogenesis is often characterized by enhanced cell proliferation

Fig. 3. Example of 4D CT where respiratory cycle irregularities have produced significant interbed mismatches near the base of the lung.

and transformation, and elevated levels of choline and choline kinase activity in certain neoplasmic dieases have motivated the development of positron-labeled choline analogs for noninvasive detection of cancer using PET.[41] Choline acts as a precursor for the biosynthesis of phospholipids, *e.g.*, phosphoatidylcholine, the major components of cell membrane. Several preliminary studies have demonstrated the potential of the new tracer for prostate cancer and many other cancers.[37,41,48]

Biologically conformal radiation therapy (BCRT)

The current 3DCRT or IMRT inverse planning is typically aimed at producing a homogeneous target dose under the assumption of uniform biology within the target volume. In reality, it is well known that the spatial biology distribution (*e.g.*, clonogen density, radiosensitivity, tumor proliferation rate, functional importance) in most tumors and sensitive structures is heterogeneous. Recent progress in biological imaging is making the mapping of this distribution increasingly possible. This new development opens a new avenue of research, coined BCRT.[49−53] The goal of BCRT is to take the inhomogeneous biological information derived from biological imaging into account and to produce customized nonuniform dose distributions on a patient specific basis. The simultaneous integrated boost (SIB) to elective volumes recently appearing in the literature represents a simple example of BCRT.

To establish BCRT, 3 major aspects must be addressed: (1) determination of the distribution of biological properties of the tumor and critical structures; (2) prescription of the desired dose distribution for inverse planning; and (3) inverse planning to generate most faithfully the prescribed nonuniform dose distribution. While the development of molecular imaging techniques is critically important in mapping biology distributions,

the successful integration of this information into IMRT planning through steps (2) and (3) is also indispensable to fully exploit the obtained biology information to improve patient care. With the optimistic assumption that spatial biology distributions within a patient can be reliably determined using biological imaging in the future, Yang and Xing[53] have established a theoretical framework to quantitatively incorporate the spatial biology data into IMRT inverse planning. To implement this method, they first derived a general formula for determining the desired dose to each tumor voxel for a known biology distribution of the tumor based on a linear-quadratic (LQ) model. By maximizing the TCP under the constraint of constant integral target dose, they obtained

$$D_0^T(i) = \frac{\alpha'_{ref}}{\alpha'_i}D_{ref} - \frac{1}{\alpha'_i}(\gamma_{ref} - \gamma_i)\Delta\mathrm{T} - \frac{1}{\alpha'_i}\ln\left(\frac{\alpha'_{ref}\rho_{ref}}{\alpha'_i\rho_i}\right),$$ (1)

where $D_0^T(i)$ is the desirable prescription dose at the voxel i with the tumor cell density, radiosensitivity, and proliferation rate given by $(\rho_i, \alpha_i, \gamma_i)$, and D_{ref} is the reference dose for the voxel with reference radiobiological parameters $(\rho_{ref}, \alpha_{ref}, \gamma_{ref})$. For a given disease site, the radiation dose used in current clinical practice with "intent to cure" can be used as a good starting point in selecting the value of D_{ref}. The relation is quite general and can be used as prescription dose to guide an arbitrary inverse planning objective function aimed at producing a customized dose distribution in accordance with the spatial biology information.

INTRA-FRACTION ORGAN MOTION: MANAGING THE RESPIRATORY MOTION

Components affecting the reproducibility of target position during and between subsequent fractions of radiation therapy include the displacement of internal organs between fractions and internal organ motion within a fraction. Depending on the disease site, these components contribute differently to the margins that are to be added around the CTV to ensure adequate coverage. In the thorax and abdomen, intra-fraction internal anatomy motion due to respiration is a principal cause for large safety margins. Motion can distort target volumes and result in positioning errors as different parts of the tumor move in and out of the image window with the patient's breathing cycle. Several studies, conducted to examine the extent of diaphragm excursion due to normal respiration, reported the range of motion from ~0.5 to 4.0 cm in the superioinferior direction. As a consequence of a significant margin added around the CTV, a large amount of normal tissue surrounding the CTV is irradiated. Accounting for such motion during treatment has the potential to reduce margins, leading to reduced radiation toxicity and risk of treatment-induced complications, and yielding room for dose escalation.

A complete solution compensating for respiratory motion should ideally start at the simulation stage. There have been several studies to characterize the amplitude, phase and periodicity of organ motion[54–56] using fluoroscopic x-rays, ultrasound,[57,58] and magnetic or RF markers.[59,60] The development and deployment of spiral and multi-detector CT scanners have made practical the acquisition of time-resolved or 4D CT images. The reconstructed images acquired with patients in treatment positions provide 4D models upon which geometric as well as dosimetric computations can be performed. 4D PET is also becoming clinically available.[61–63] Treatment-wise, respiratory gating technology and tumor tracking techniques to synchronize delivery of radiation with the patient's own respiratory cycle are under intensive investigations.

4D CT imaging

A 4D CT can be either prospective or retrospective. In the former case, the scanner collects images at only one of the breathing phases of the patient instead of scanning continuously. The retrospective 4D CT scan results in multiple image sets, corresponding to different breathing phases of the patient, and consists of 3 relatively orthogonal processes[64–68]: recording of respiratory signal(s), acquisition of time-dependent CT projection data, and construction of a 4D image from these data. The first objective can be achieved by tracking a surrogate of respiration-related organ and tumor motion, such as tidal volume measured with a spirometer,[66,69] chest expansion monitored by a pneumatic bellows,[70] or a reflecting external marker placed on the abdomen and tracked with a camera.[64] Time-dependent CT data can be acquired by oversampling in either helical or cine mode, and constructing several CT slices over the full respiratory cycle at each axial location.[67,71] Finally, the respiratory signal and CT data must be combined into a 4D series, providing a CT volume at several points throughout the respiratory cycle. In this section, we will focus primarily on the implementation of 4D CT provided by the Varian Real-time Position Management (RPM) camera/software and the GE Discovery ST multislice PET/CT scanner.

4D CT patient setup proceeds along the same lines as a standard 3D CT exam. The patient is immobilized on the scanner bed, and aligned using room and scanner lasers. Sagittal and coronal scout images are used to verify patient positioning, and the setup is adjusted as necessary. At this stage of the setup, the 4D procedure begins to diverge from the 3D exam.

The RPM system consists of an infrared source, CCD camera, and a reflecting block. The block is attached to the patient's abdomen, typically just inferior to the xiphoid process, and the anterioposterior motion of the block is captured by the camera. This motion is analyzed in real-time by Varian software on a computer connected to the RPM camera. The breathing pattern is recorded for the duration of the scan, and is referred to as the "respiratory trace." Once the scan has finished, the software retrospectively computes the phase at each point of the respiratory trace by determining the location of the peaks at end-inspiration, and assigning percentages to interpeak points based on a linear interpolation of the peak-to-peak distance. For example, under this scheme, end-inspiration occurs at 0%, while end-expiration typically appears near 50–60%. The peak-to-peak distance can vary between respiratory cycles, as can the position of end-expiration with respect to end-inspiration.

Irregularities in a patient's respiratory pattern can often be reduced by encouraging the patient to breathe calmly and consistently, and then relying on the patient's compliance during the scan. If this free-breathing approach is insufficient, the RPM software can provide audio coaching in the form of a "breathe in, breathe out" recording, which is manually or automatically timed to the patient's natural rhythm. Some groups have used video feedback either alone or concurrently with audio instructions.[72] While audio and video coaching can help by stabilizing the respiratory period, amplitude and baseline, they can complicate matters for patients with compromised respiratory function, who find it difficult or impossible to maintain a regular rhythm. Another solution is active breath control (ABC)[73–75] which uses modified ventilator equipment to control the airflow, albeit at the (possibly significant) expense of patient comfort.

Once a sufficiently regular breathing pattern has been established, the CT data is acquired in "cine" mode. This is a step-and-shoot technique, whereby the gantry rotates several times at each bed position to acquire data over the full respiratory cycle. The raw data is partitioned into bins corresponding to a user-selected time interval (typically less than 1/10th the average cycle), and CT slices are automatically reconstructed from these bins. Because several respiratory points are sampled at each bed position, a 4D CT scan can take several times as long as a corresponding 3D CT, resulting in typically 1500–3000 CT slices for a 20–40-cm axial FOV.

The respiratory and scan data are combined at a separate computer, the Advantage Workstation (AW) (GE Medical Systems), which uses the respiratory trace to sort the oversampled CT slices according to their phase. The AW does perform the phase calculations, but rather relies on the phase stamp computed by the RPM during the creation of the respiratory trace file. Missing phases for any couch position are replaced with their nearest neighbor, providing a sorted image without any phase gaps. The user can navigate through the data in each axial direction, similar to standard viewing software, but can also scroll through the respiratory phases from end-inspiration to end-expiration. Individual phases can be subsequently extracted, or combined into averaged or minimum/maximum intensity projections, and exported to planning software in the form of standard
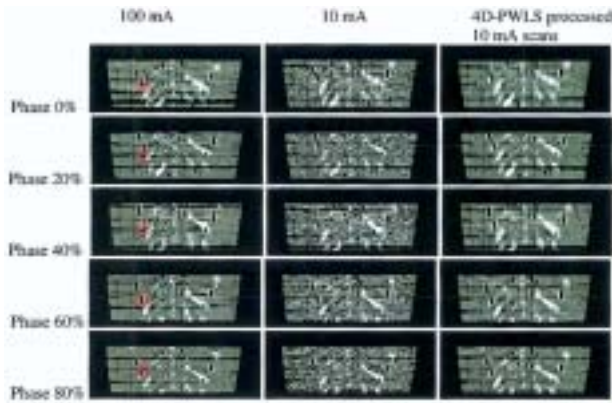
Fig. 4. Motion phantom study for the 4D-PWLS method with the thorax phantom. The left and middle columns are the original phases obtained from the GE Advantage Workstation, for 100 mA and 10 mA, respectively; the right column shows the 10-mA phases after 4D-PWLS processing. The red rectangles represent the selected ROI for calculation of SNRs, each of which contains $5 \times 5 \times 5$ voxels. PWLS smoothed 10-mA scan resulted in more than 2-fold increase in the SNR for every phase of the periodically moving phantom. Similar results were obtained in a patient 4D CT study.

DICOM series. These exported image series form the basis of 4D treatment planning.

Unresolved issues in 4D CT

The AW sorts the data by phase rather than amplitude. If the breathing were perfectly regular from cycle to cycle, then phase- and amplitude-based sorting would give very similar results. The problem arises when there is variation in amplitude, period, or baseline, or when the onset of end-expiration does not occur at the same point each cycle. When these inconsistencies arise, the sorted CT images may contain mismatch artifacts at the interface between bed positions (see Fig. 3). Recent studies have investigated amplitude-based binning as an alternative to the phase-based approach, and it appears that amplitude sorting can improve image quality in many cases.[76–78] Other researchers have matched adjacent CT slices without using a respiratory trace, by maximizing the continuity of CT units integrated over regions of interest.[71] Yet another promising approach involves interpolating the CT data continuously between end-cycle peaks using deformable models.[79]

A second issue arises in the correlation between external fiducial movement and tumor/organ motion. Amplitude ratios between fiducial and tumor displacement may vary from cycle to cycle, and thoracic and abdominal points may involve relative phase shifts.[54,80] These shifts may be especially crucial for tumors near the lung, where hysteresis is prevalent. Finally, larger organs such as the liver can experience substantial deformation during inspiration and expiration, which may not be adequately captured by rigid-body interpolation between points in the respiratory cycle

Finally, even if the 4D CT images have been acquired without problem, there remains the issue of reproducibility at treatment.[81] If treatment planning and delivery are based on 4D CT, there is an implicit assumption that anatomic motion during treatment will match the tumor and organ motion observed during setup. This assumption can be checked to some degree through frequent gated or breath-hold portal imaging.[82] On the other hand, it is reasonable to assume the patient will relax over time, so that their breathing becomes shallower or changes tempo. Indeed, studies have demonstrated that some patients exhibit systematic respiratory changes over a several-week course of radiation therapy, even with visual and audio coaching.[83] These issues strike at the heart of IGRT, and provide a fertile ground for research.

4D CT usually delivers more radiation dose than the standard 3D CT, because multiple scans at each couch position are required to provide the temporal information. We have developed a method to perform 4D CT scans at relatively low current, hence reducing the radiation exposure of patients.[68] To deal with the increased statistical noise caused by the low current, we proposed a novel 4D penalized weighted least square (4D-PWLS) smoothing method, which can incorporate both spatial and phase information. The 4D images at different phases are registered to the same phase via a deformable model, whereby a regularization term combining temporal and spatial neighbors is designed. The proposed method was tested with phantom experiment (see Fig. 4). for an example) and patient study, and superior noise suppression and resolution preservation were observed.

4D PET and related issues

4D PET poses a problem distinct from 4D CT, in that signal is inherently limited by the tolerable patient dose. The result is that any PET scan requires a significant amount of time per bed position (usually a few minutes) to acquire sufficient data to produce a good image. This limitation makes it difficult to partition PET data with the same time resolution possible in 4D CT, but nonetheless, acquisition methods are clinically available to obtain PET images at end-inspiration or end-expiration. The most common solution is to gate the PET scan at the desired respiratory end-point, and reconstruct a single bin of gated data.[84–86]

Patient setup proceeds in the same manner as an ungated PET scan, and a CT image is acquired for attenuation correction just prior to the PET. At this point, the RPM system monitors patient breathing by tracking the reflecting block, and the acquisition trigger is set by the user to occur at some given point (say, end-inspiration) in the cycle. Each time the RPM camera determines that the reflecting block (and, by extension, the patient's respiration) reaches this point in the respiratory cycle, a trigger is sent to the scanner, and data accumulation is initiated. Gated PET differs fundamen-

tally from the 4D CT protocol, by elevating the RPM system to this active role in data acquisition.

In gated mode, the user is able to select both the width of the acquisition window and the number of sequential bins to record each respiratory cycle. The bin width directly affects image quality, because the signal-to-noise ratio within an image asymptotically approaches the square root of the signal level.[87] Multiple bin acquisition allows the capture of the full respiratory cycle in several bins, offering the possibility of retrospectively sorting into 2 or more respiratory phases. Each time the RPM trigger is received, data is directed to the initial bin, and then to the remaining bins sequentially until the next trigger. This process continues for the duration of the scan. Ideally, the scan duration would be chosen such that the first bin (the respiratory point of most interest) would accumulate as many data points as a comparable ungated scan (*i.e.*, divide the bin width by the duty cycle). In reality, because this would lengthen the typical PET scan by a factor of 4 or 5, practical clinical considerations may require the gated scan to be shortened, with corresponding image degradation.

Once the scan has finished, it is possible to associate each bin (beyond the first bin) with a corresponding point in the respiratory cycle. Because the respiratory trace is recorded by the RPM, it is a relatively simple matter to analyze the respiratory motion offline and make this correspondence. It is also possible to retrospectively combine multiple bins into a single bin, merging all the data to create an effectively ungated scan. However, these methods are not yet available from the vendor as a clinical tool, and must be performed by the user in the context of research efforts. Once the desired bin has been selected, its data can be reconstructed using the vendor-supplied filtered backprojection or OS-EM algorithms. The image results can subsequently be exported to treatment planning systems for review, similar to ungated PET series.

A salient point in the PET reconstruction process is the specification of the attenuation correction map. The current clinical design uses the CT scan acquired just prior to the PET specifically for this purpose. This attenuation correction CT can be an acquired during either free breathing or breath-hold. Some research has indicated that PET reconstructions can be quite sensitive to distortions in the attenuation correction map,[88–90] and investigations are ongoing into the use of 4D CT or other models to accurately account for attenuation.[61,91] On the Varian/GE system, this requires selecting the appropriate images from the 4D CT on the AW, sending these series back to the scanner, generating the attenuation correction maps for each 4D PET bin, and then reconstructing each bin separately. Once again, this is a research solution, and not yet available from the vendor for clinical use.

Combining 4D PET with 4D CT and enhancement of the performance of 4D PET with post-acquisition data processing

Once the 4D PET has been acquired (either a single phase, or perhaps several), it is possible to create a 4D PET/CT.[61] This involves manually selecting the PET and CT images with corresponding respiratory phases (or amplitudes), and fusing them on viewing/planning software. We have recently developed a 4D-4D image registration algorithm, which allows us to automate the process. If the CT and PET scans are acquired with the same patient position on the same exam, then the process is a particularly simple hardware-based registration. On the Eclipse treatment planning system, for example, 2 images (not just PET/CT, but other modalities as well) can be automatically fused if they share the same DICOM coordinates. If the DICOM coordinates are not identical, the registration is more difficult, requiring manual or automated shifts and rotations to match anatomical landmarks or fiducials. Fusion may be additionally complicated by organ deformation[92,93] (see Rigid and Deformable Image Registration Section below). At the present time, PET/CT hardware fusion for ungated scans is well established and readily available within the clinical setting.[13,14] 4D PET/CT registration, however, remains primarily within the research domain.

The major issue in 4D PET is the lack of statistics. Because the collected photons are divided into several frames, the quality of each reconstructed frame is decreased with increasing number of frames. The increased noise in each frame heavily degrades the quantitative accuracy of the PET imaging. We have recently developed 2 corrective methods to enhance the performance of 4D PET. The first method, coined "retrospective" stacking (RS),[62,63,94] combines retrospective amplitude-based binning of data acquired in small time intervals, with rigid or deformable image registration methods. Unlike gating techniques, RS uses data along the entire respiratory cycle, thereby minimizing the need for lengthened scans while providing a 4-dimensional view of the region of interest.[62,63] In the second approach,[94] we reconstruct each frame with all acquired 4D data by incorporating an organ motion model derived from 4D-CT images by modifying the well-known maximum-likelihood expectation-maximization (ML-EM) algorithm. During the processes of forward- and backward-projection in the ML-EM iterations, all projection data acquired at different phases are combined together to update the emission map with the aid of the deformable model, the statistics are therefore greatly improved. Both phantom and patient studies have indicated promising potential of the 2 methods.

Radiation treatment planning based on 4D information

How to maximally utilize the time-resolved image information derived from 4D CT or PET/CT represents one of the challenges in IGRT. In reality, the information
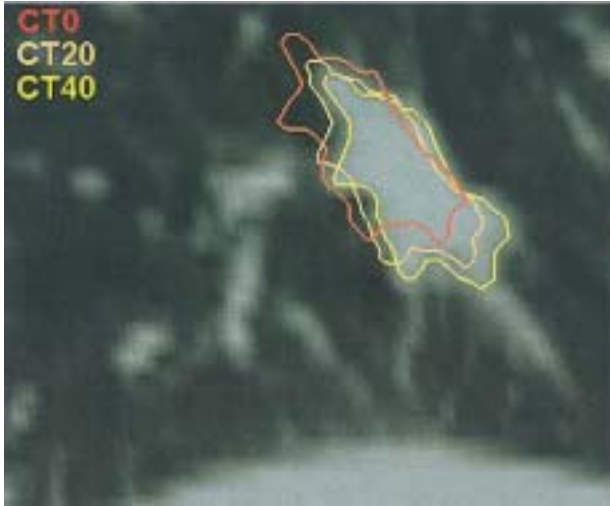
Fig. 5. Tumor contours for 3 breathing phases. The contours labeled as CT20 and CT 40 were produced by applying the deformation field on the tumor contours delineated in CT0. The "trajectories" of the tumor boundary pictorially show the extent of tumor movement and allow us to specify patient specific margin in accounting for the intra-fraction organ motion.

can be integrated into radiation treatment planning and delivery at different levels. At the lowest level, the 4D images can be employed to determine the extent of tumor movement on a patient specific basis and the information can then used to design the CTV margin and the radiation portals to accommodate the motion. Figure 5 shows an example of lung patient, in which tumor boundaries at 3 distinct respiratory phases are plotted. We have referred to this type of treatment as "3.5-dimensional" radiation therapy. The 4D information can also be used for guiding breath-hold or gated radiation therapy. There is also strong interest in using the 4D data to establish a 4D patient model and then to carry out a 4D radiation therapy plan. These are the subjects of the following 2 sub-sections.

Breath-hold and respiratory gating

Various methods have been worked out to counteract respiratory motion artifacts in radiotherapy imaging. Among them are breath-hold, respiration gating, and 4D or tumor-tracking techniques.[55,56,73,75,95] Breath-hold techniques either actively or passively suspend the patient's respiration and treat the patient during this interval. Deep inspiration breath-hold, active breathing control (ABC) (which forces shallow breathing and thereby "freezes" the tumor motion for a small part of the treatment time[73]), and self-held breath-hold are suitable for different types of therapy targeting different cancers. Different types of equipment, such as stereotactic frames, fiducial tracking systems, timers, respirometer, RPM, or interlocks, may be needed depending on the method of breath-hold.

Respiration-gating methods involve tracking the pa-

tient's natural breathing cycle and periodically turning the beam on when the patient's respiration signal is in a certain phase of the breathing cycle (generally end-inhale or end-exhale). The patient's respiration is continuously monitored and the beam switches off as the tumor moves out of the target range. Gated radiation therapy can offset some of the motion but requires specific patient participation and active compliance. In gated treatment, it is required that the CT images used for treatment planning faithfully represent the actual treatment situation. While gated CT acquisition at the treatment respiratory phase is possible, our gating protocol proceeds by picking up the CT data at an appropriate phase from the patient's 4D CT acquired using the method described above. The gating interval is typically centered at end-expiration because of the increased reproducibility at this point, and spans 20–30% of the breathing period to provide a reasonable duty cycle. Treatment plans are optimized for this phase range by planning on an averaged composite of the scans within the interval, and using maximum- and minimum-intensity pixel views to incorporate intra-gate margins. The averaged, maximum-intensity and minimum-intensity composites for a lung patient are displayed in Fig. 6.

Tumor tracking

Similar to the establishment of a 3D geometric modeling based on traditional CT data, the availability of 4D imaging information makes it possible to build a patient specific 4D model. Figure 7 shows the the 4D model for a lung patient.[79] In obtaining the models, a BSpline deformable registration technique (see Rigid and Deformable Image Registration section below) was used to register different phases of the 4D CT. Ideally, organ motion represented by the 4D model can be incorporated into the radiation treatment plan optimization to overcome the adverse effect of respiratory motion on IMRT delivery.[96] A few groups[95–100] have explored the feasibility of MLC-based tumor tracking. However, the interplay between different phases has been ignored during the plan optimization in most of these studies. Webb has presented a technique to model the dosimetric effect of elastic tissue movement when modulated beams are delivered.[101] In general, the quadratic inverse planning objective function becomes

$$F = \sum_t \sum_k \cdot \sum_i w_k \left[d_p^k - \sum_t d_i^k(\vec{r}, t) \right]^2 \qquad (2)$$

where d_p^k is prescribed dose for kth structure, w_k is the importance factor, and $d_i^k(\vec{r}, t)$ is the calculated dose in voxel i at time t, and the summation over t represents the integral dose to ith voxel. For 4D planning, it is necessary to know the path of each material coordinate during the treatment, which involves registering the voxels in different respiratory phases. This can be achieved by using a deformable registration algorithm. The optimization of the above objective function or alike[95,102–106]
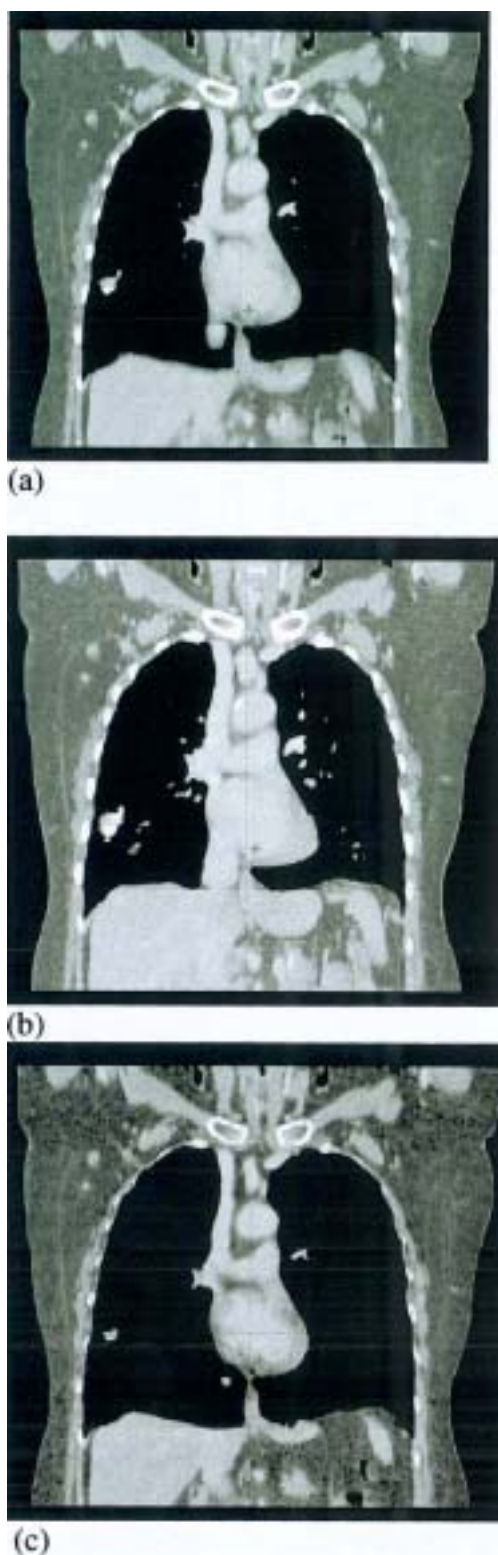
Fig. 6. Composite scans of a 4D CT lung patient. (a) Average pixel; (b) maximum-intensity pixel; (c) minimum-intensity pixel. The maximum-intensity pixel composite reveals the motioextent of hyperdense tissue (*e.g.*, lung tumor), while the minimum-intensity pixel view provides the motion range of hypodense regions (*e.g.*, lung air volume).

can proceed in a similar fashion as conventional 3D inverse planning to derive the optimal trajectories of the movements of the MLC leaves. An aperture-based optimization[107–109] seems to be more adequate for dealing with the organ motion.[96]

4D methods propose to track the tumor with the radiation beam as the tumor moves during the respiration cycle. These techniques require acquisition of some form of respiration signal (infrared reflective markers, spirometry, strain gauges, video tracking of chest outlines, and fluoroscopic tracking of implanted markers are some of the techniques employed to date), which is assumed to be correlated with internal anatomy motion. Fluoroscopy and the cine model electronic-portal-imaging device (EPID) have been proposed as a means for real-time guidance.[110,113] While tumor tracking seems to be the ultimate goal of 4D radiation therapy, the real challenge is clarifying whether the 4D model is repeatable at the time of fractionated treatments, and determining how to correctly synchronize the MLC movements with the patient breathing. Real-time imaging and/or adaptive approaches will likely play a role in this aspect and the issue will surely need more research for many years to come.

INTER-FRACTION ORGAN MOVEMENT

Current techniques in dealing with inter-fraction organ movement

Uncertainty in patient setup has long been known as a limiting factor to conformal radiation therapy. Currently, the accuracy of patient setup is verified by megavoltage (MV) radiograph acquired with either radiographic film or EPID.[114,115] The patient's bony landmarks are used to guide patient alignment. Poor soft tissue contrast and often unclear projection of the bony anatomy are major problems of the approach. To improve the situation, planar kV x-ray imaging has been implemented in a variety forms.[110–113] While these systems show significantly increased contrast for bony structure differentiation, observing soft-tissue detail remains problematic and correction of daily organ motion is still challenging. Attempts have been made to use CT imaging to facilitate the patient setup process. Along this line, the offline adaptive-radiation-therapy (ART) strategy[116] and in-room CT approach[117] have been studied. The former method aims to partially compensate for organ motion by carrying out multiple CT scans in consecutive days in the first week of treatment. The image data are then employed to construct a patient specific PTV model from the composite of the CTVs with inclusion of statistical variations of the observed motions. While beneficial, the approach is hardly an ideal solution for dealing with the inter-fraction organ motion. It relies on establishing a statistical ensemble of all possible setup scenarios under a strong assumption that a limited number of off-line CT scans can ade-
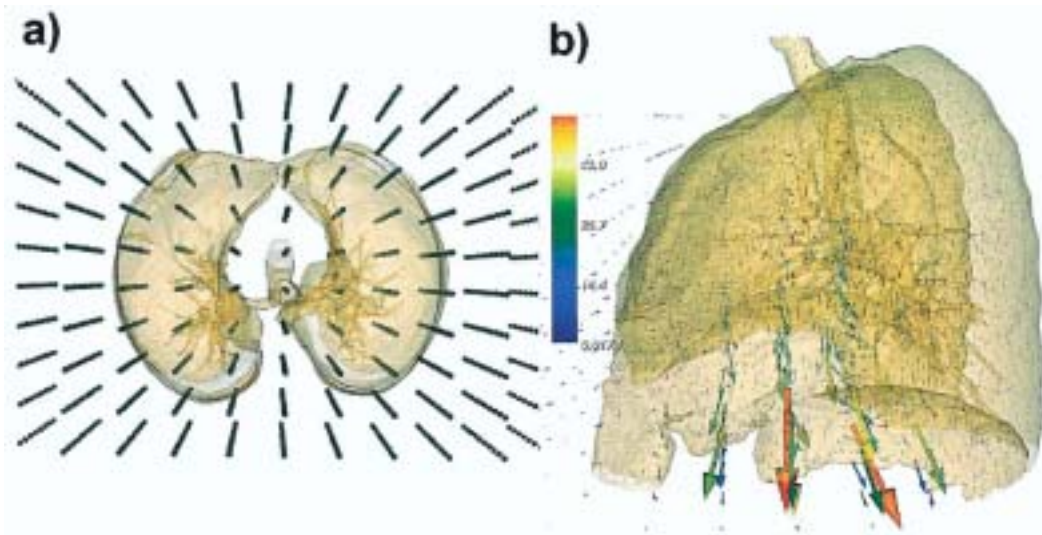
Fig. 7. (a) The BSpline grid superimposed on lung contours. (b) On each node, deformation is represented by arrows, where arrow length is proportional to the deformation.

quately describe the inherently complex, often unpredictable inter-fraction organ motion. Even when it is achievable, the ART margin is not optimized on a daily basis and there is still room for further improvement. An integrated CT/LINAC combination, in which the CT scanner is located inside the radiation therapy treatment room and the same patient couch is used for CT scanning and treatment (after a 180° couch rotation), should allow more accurate correction of interfractional setup errors. Some major radiotherapy vendors provide options to install a CT scanner in the treatment room. The overall precision of EXaCT Targeting™ from Varian has been evaluated by Court *et al.*[117] However, the approach assumes a fixed relationship between the LINAC isocenter and the CT images and relies heavily on the mechanical integrity of the 2 otherwise independent systems. Increased capital cost and prolonged imaging and treatment are other concerns.

Other patient localization techniques available include ultrasound-based methods, video-based surface tracking, on-board cone-beam CT or kV x-ray imaging, CyberKnife and Tomotherapy, etc. For prostate radiation therapy, on-line ultrasound imaging has gained substantial interest[118–120] but in practice has been found susceptible to subtle sources of error and inter-user variability. On-board CBCT holds promise to become a robust integrated on-line imaging technology that can yield unambiguous soft-tissue detail at the time of treatment. Furthermore, CT numbers correlate directly with electron density, thereby providing the potential for reconstruction of the actual dose delivered on a daily basis, in addition to simple anatomic structure alignment. The details of emerging CBCT will be presented in the next section. The robotic CyberKnife™TM from Accuray Inc. (Sunnyvale, CA) represents another promising tech-

nology. The system has a feedback mechanism in which motion of the CTV, determined through the Accutrak infrared-x-ray-correlated imaging system, can be fed back to the robot to track the CTV.[121] However, while this improves the duty cycle, there is a finite time between measuring tumor position and arranging the compensation for motion. Helical tomotherapy is an alternative means of delivering IMRT using a device that combines features of a linear accelerator and a helical CT scanner.[122] The commercial version, the HI-ART IITM, can generate CT images using the same MV radiation beam that is used for treatment. Because the unit uses the actual treatment beam as the x-ray source for image acquisition, no surrogate telemetry systems are required to register image space to treatment space. Objective measures of noise, uniformity, contrast, linearity, and spatial resolution, and comparison with that of a commonly utilized CT simulator, have recently performed by Meeks *et al.*[123]

CBCT for patient localization

CBCT based upon flat-panel technology integrated with a medical linear accelerator has recently become available from linac vendors for therapy guidance. The volumetric images may be used to verify and correct the planning patient setup in the linac coordinates by comparing with the patient position defined in treatment plan. Both kV and MV beams have been utilized for the application. The former typically consists of a kV-source and flat-panel combination mounted on the drum of a medical accelerator,[124] with the kV imaging axis orthogonal to that of MV therapy beam. The fan-beam and cone-beam MV CT in clinical applications have been reported by Meeks *et al.*[123] and Poulliot *et al.*[125], respectively. It appears that the MV images contain sufficient
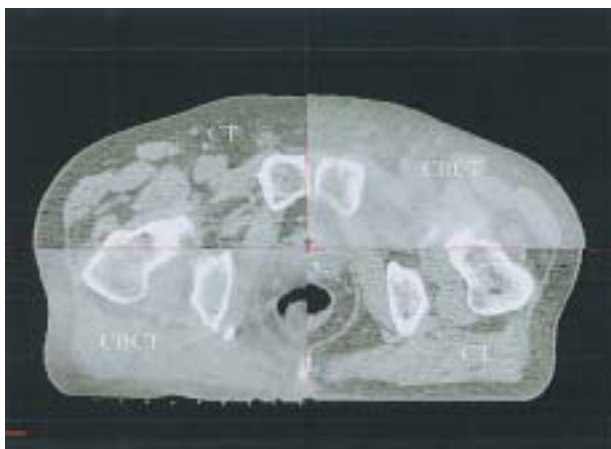
Fig. 8. The fusion of the 2 types of CT and CBCT images for a prostate case.

resolution of bone and air cavities to register them to structures in the planning CT with millimeter precision.[124,125]

Currently, CBCT is primarily used for guiding the patient setup.[126,127] The procedure is not much different from the current patient treatment, other than the fact that the AP/LAT portal images are replaced by volumetric data. In Fig. 8, we show 3D CBCT images of a prostate case in one of the fractional treatments fused with the patient's planning CT image. It is seen that soft-tissue structures and boundaries are visible to varying degrees in the CBCT images. The patient has implanted fiducials, which show up on both CBCT and planning CT. Our experience indicates that the cone beam data can clearly reveal setup error, as well as the anatomical deformations and other physiological changes. During the patient setup process, the 3D CBCT images are registered with the planning CT data through the use of either manual or automated 3D image registration software that calculates shifts in x-, y-, and z-directions (depending on the manufacturer, rotations can also be included). The movements determined during the registration represent the required setup corrections that should be applied to the patient. Both phantom and patient studies from our group have shown that the volumetric imaging is superior to the conventional MV or kV AP/LAT patient setup procedure. We note that, if only translational shifts are permissible, the level of improvement is generally within 2 mm as compared with kV AP/LAT setup procedure (2D/2D match). However, CBCT can readily detect rotational errors that may otherwise be missed by the 2D/2D match. In Fig. 9, we show the localization image for a head phantom with kV/kV 2D/2D match and 3D/3D match (CBCT/planning CT). The latter approach was found to be sensitive enough to identify a rotational error as small as 2°.

In practice, much effort is needed to improve the robustness and efficiency of the volumetric image regis-

tration process. Furthermore, to fully utilize the volumetric data, a new paradigm with seamlessly integrated simulation, planning, verification, and delivery procedure is urgently needed. Until this is realized clinically, the volumetric imaging is nothing but an expensive extension of the already functional planar verification approach. The capital cost and other related overheads do not seem to justify the marginal benefit if the volumetric data is simply used for determining the patient shift in the space. However, one should not underestimate the potential of the volumetric imaging for the future of radiation therapy, as it opens a new avenue (perhaps the only avenue), for us to realize the planned dose distribution with high confidence in clinical settings.

A few groups are working on deformable model based segmentation and patient setup procedures.[93,126–128] When deformable registration is used, there are a few options to achieve the registration depending on whether the primary aim is to match soft-tissue, or to align 3D bony structures. In Fig. 10, we show a patient's CBCT and planning CT registration results using different registration schemes. The multiple choices result from the fact that the dimensionality of the patient data is much greater than that in the patient setup procedure, and suggest that deformable registration is not the ultimate solution to volumetric image-guided radiation therapy. Nonetheless, the technique improves the current method,[127] because it partially takes into account organ deformation by achieving the closest overlay match possible between the planning and CBCT data sets according to our clinical objective, and serves as a useful interim solution before a better integrated approach becomes available.

CBCT-based dose verification

Another important application of on-board volumetric imaging is verification of dose delivery. We have recently evaluated the accuracy of kV CBCT-based dose calculation and examined if current CBCT is suitable for the daily dose verification of patient treatment.[129,130] A CT-calibration phantom was first used to calibrate both conventional CT and CBCT. CT and CBCT images of the calibration phantom, an anthropomorphic phantom and 2 patients (a lung and a prostate case) were then acquired for this study. Our results indicated that the imperfect quality of CBCT images has minimal impact ($< 3\%$) on the dosimetric accuracy when the intra-fractional organ motion is small. When intra-fractional organ motion is large and motion artifacts is severe (*e.g.*, in the case of lung cancer), the dosimetric discrepancy due to the poor image quality of current CBCT was found to be clinically significant. Furthermore, in the latter case, we found that it is possible to use a deformable registration algorithm to map the corresponding electron density information from planning CT to CBCT and then to proceed with conventional dose calculation.
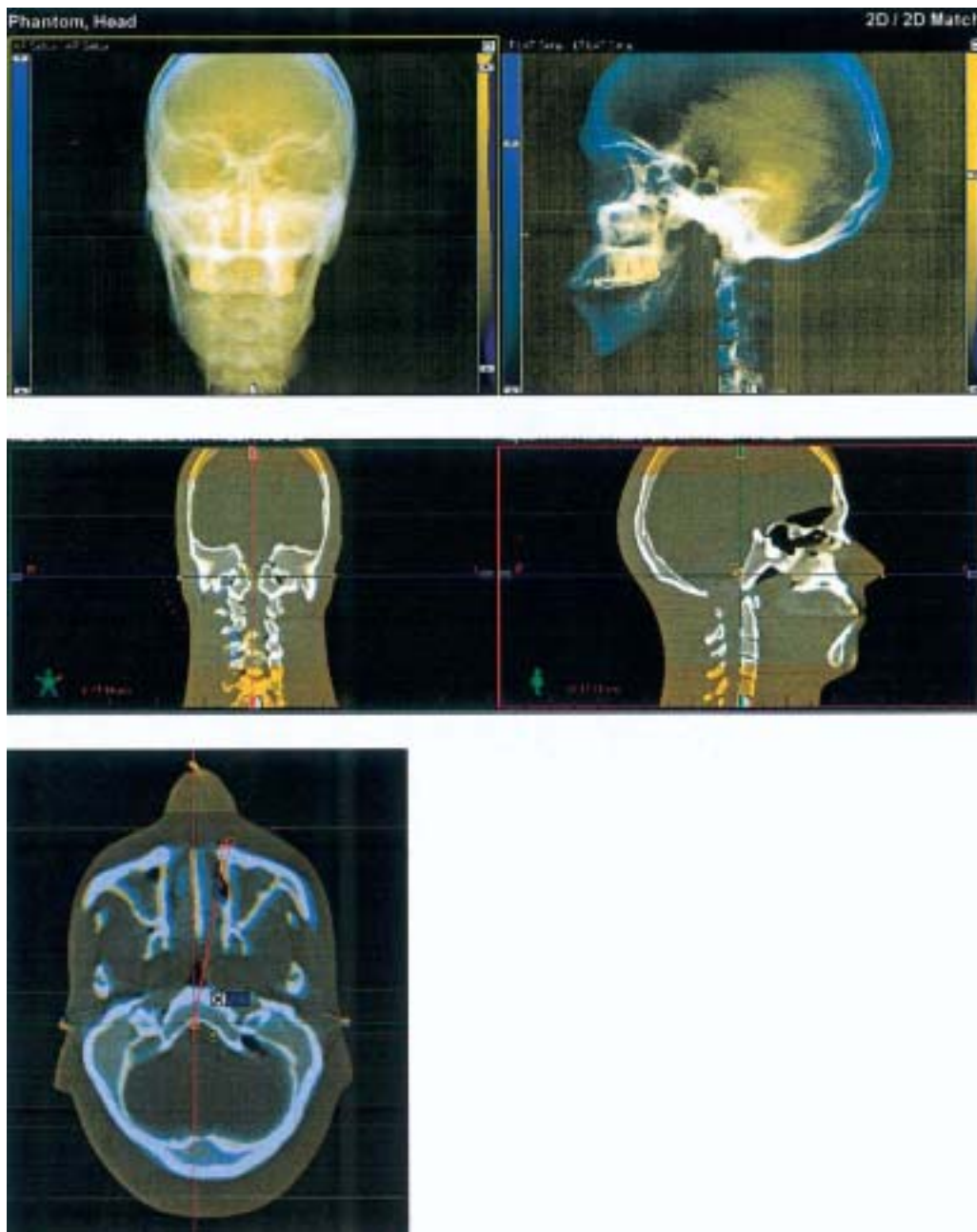
Fig. 9. Setup localization image for head phantom with kV/kV 2D/2D match (top) and 3D/3D CBCT match (middle).
The image shown in the bottom panel illustrates that the CBCT is a sensitive technique capable of picking up a 2°
rotational miss-match between the planning CT and CBCT.

Respiratory motion artifacts in CBCT

Superior to the common approaches based on 2 orthogonal images, CBCT can provide high-resolution 3D information of the patient in the treatment position, and thus has great potential for improved target localization and irradiation dose verification. In reality, however, scatter and organ motion are 2 major factors limiting the quality of current CBCT. When CBCT is used in imaging thorax or upper abdomen of a patient, respiration induced artifacts such as blurring, doubling, streaking, and distortion are observed, which heavily degrade the

image quality, and affect the target localization ability, as well as the accuracy of dose verification. These artifacts are much more severe than those found in conventional CT exams, in which each rotation of the scan can be completed within one second. On the contrary, in CBCT scan, the gantry rotation speed is much slower, typically 40 seconds to 1 minute for a full 360° scan in acquiring the projection data, which is more than 10 breathing cycles for most patients. In Fig. 11, we show the influence of the same motion on a regular "fast" CT scanner and CBCT for a motion phantom, where it is clearly seen
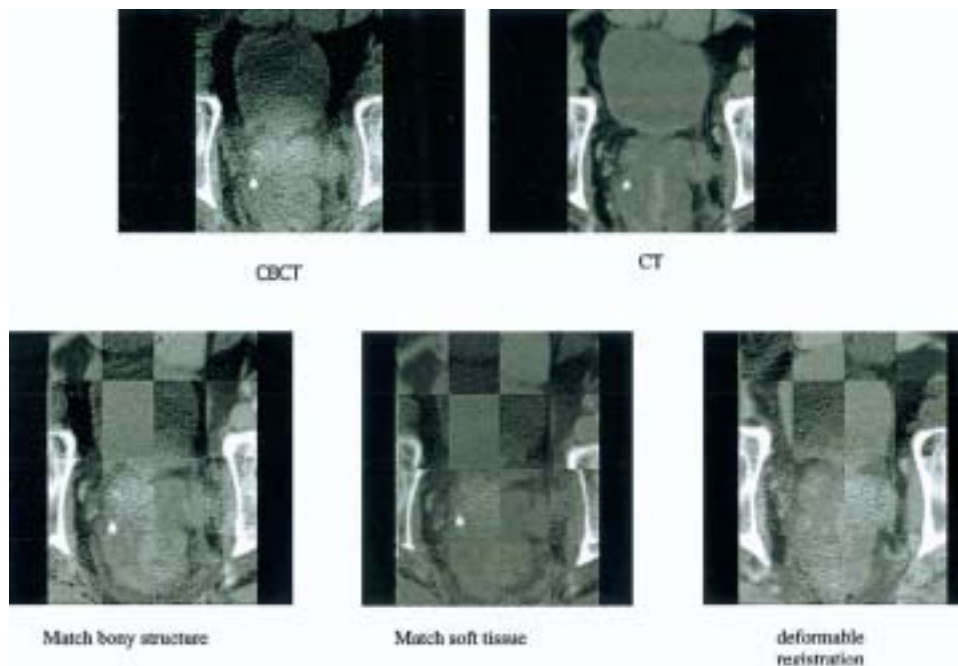
Fig. 10. Image registration of CBCT and planning CT based on bony structure matching, soft tissue matching, and deformable registration. Different matching techniques emphasize on different aspect of the multidimensional problem.
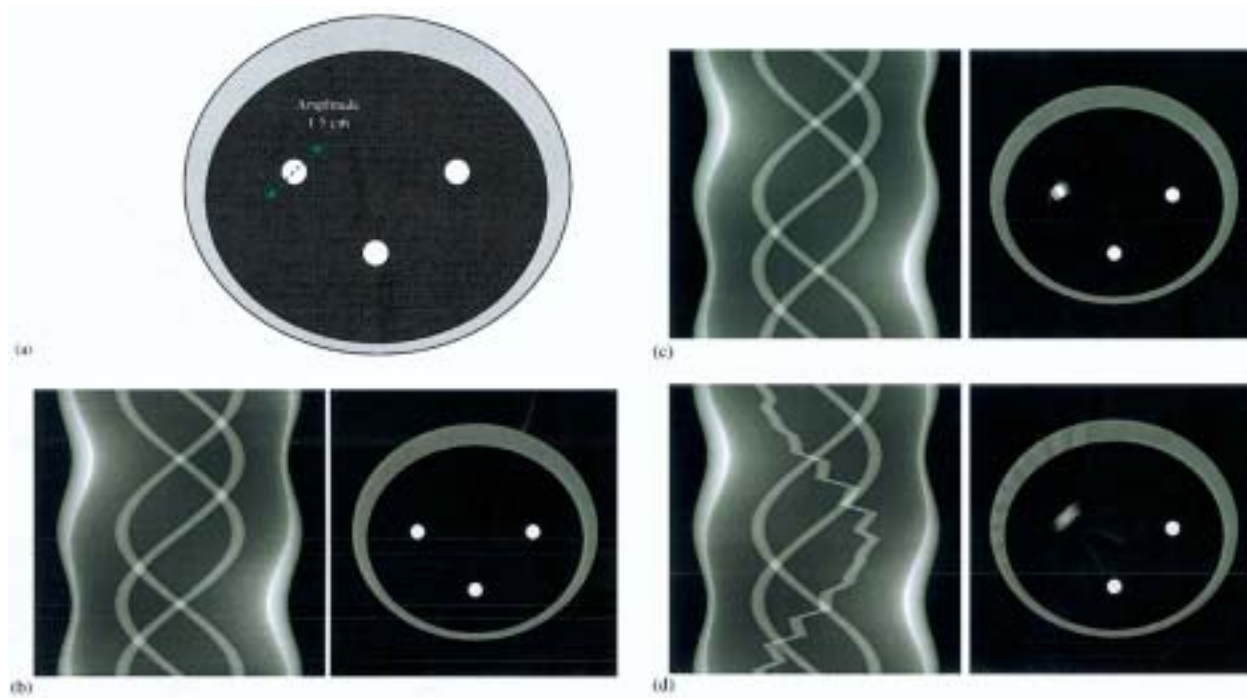
Fig. 11. (a) Motion phantom for CT and CBCT simulation study. The left circle moves diagonally with an amplitude of 1.5 cm and a period of 3.52 seconds. (b) Simulated sinograms and their corresponding reconstructed images with standard FBP algorithm when the circles are stationary. (c) and (d) show the sinograms and their corresponding reconstructed images for 1 s/rotation acquisition (conventional CT scan speed) and 40 s/rotation acquisition (on-board CBCT scan speed), respectively.
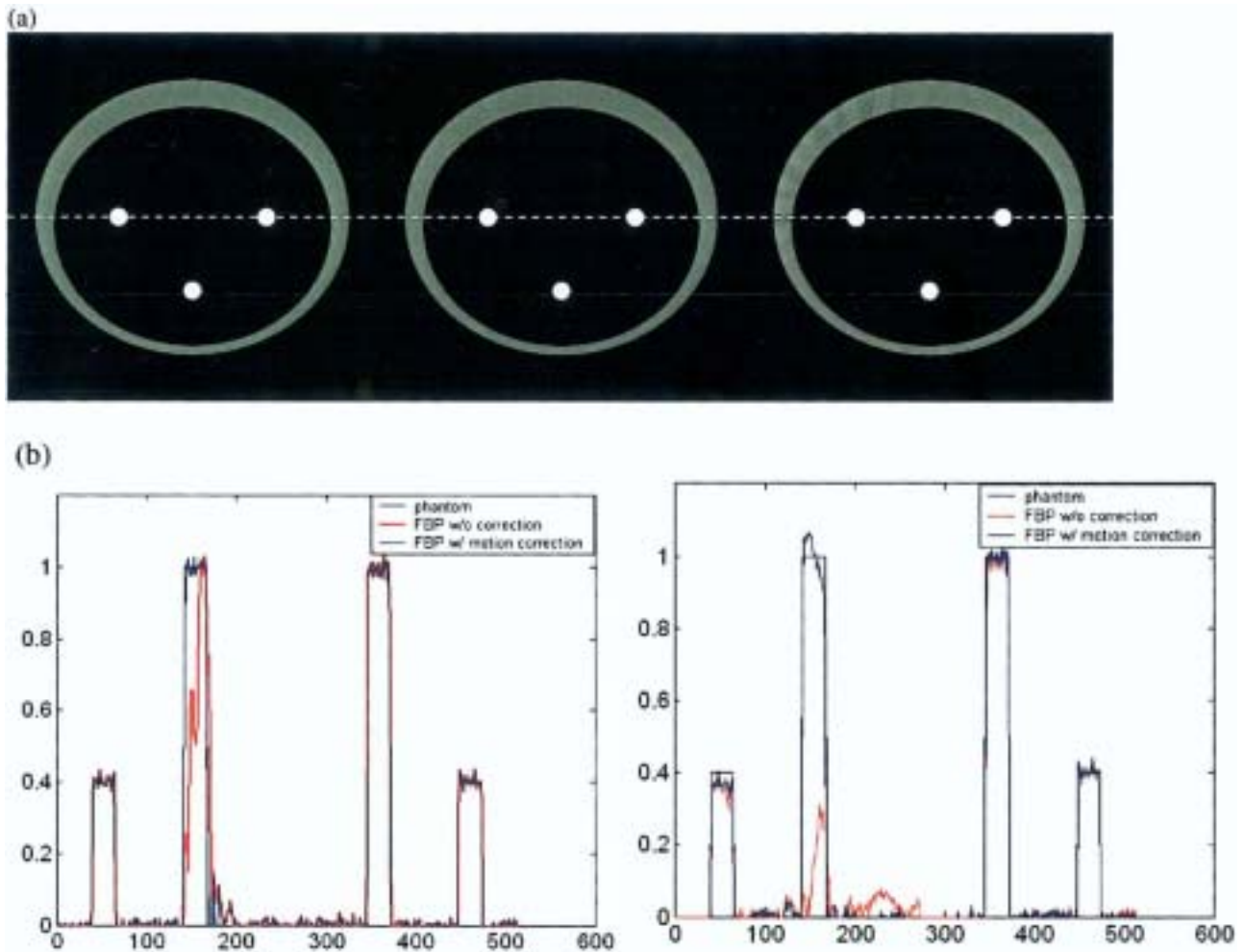
Fig. 12. (a) Phantom and images reconstructed with motion correction for CT and CBCT settings. The 3 images represent the reconstructed image of stationary phantom (left), the conventional "fast" CT (middle), and the CBCT (right). (b) Horizontal profiles through the moving circle for the reconstructed CT (left panel) and CBCT (right panel) images shown in the middle and right of (a). The profiles are in blue. For comparison, the profiles for the stationary phantom (left panel) and images reconstructed without motion artifacts removal mechanism are also plotted in each case (black and red curves, respectively).

that the motion artifacts are much greater than that in a fast scanner.

In the last decade, considerable effort has been devoted to finding solutions to remove motion artifacts and to obtain time-resolved medical images. Wang and Vannier[131] presented a patient-motion estimation and compensation technique for helical CT systems. Willis and Bresler[132] cast the motion artifact problem as a time-varying tomography problem and required special-purpose hardware to optimally sample the spatially and temporally band-limited CT signal space. A parametric model for the respiratory motion was used in MRI, and the motion artifacts were successfully reduced by modifying the reconstruction algorithm.[133] Crawford *et al.*[134] brought the concept into CT imaging, and derived an exact reconstruction formula for motion compensation for CT scans. Generally, motion correction algorithms that assume a motion model work well when the motion

conforms to the model, but have limited success when it does not. As described above, 4D CT has been developed in radiation oncology application to explicitly account for the respiratory motion. The 4D CT can be used to derive a patient-specific deformation field and then incorporated into the CBCT filtered-backprojection (FBP) image reconstruction process.[135] The algorithm was tested with simulations at different settings corresponding to conventional CT and CBCT scan protocols, with translational motion and more complex motion, and with and without Gaussian noise. In Fig. 12, we show the result for the motion phantom depicted in Fig. 11.[135] Because the motion model is directly derived from the patient images, it should be more accurate than other artificial modeling, and therefore more efficient motion correction is expected. In addition to this approach, Sonke *et al.*[136] developed a CBCT procedure consisting of retrospective sorting in projection space, similar to

that used in 4D CT. The subsets of projection data are then reconstructed into 4D CBCT dataset. To achieve a sufficient temporal resolution, however, this will require slowing down the gantry rotation. The assumption of periodicity of the respiratory motion is also necessary. Li et al.[137] have recently established a novel 4D CBCT reconstruction formalism, in which the reconstruction of a phase will consider not only the projections corresponding to that phase but also those of other phases. By incorporating information from other phases, the efficacy and quality of 4D CBCT images are substantially improved. Zeng et al.[138] proposed a method to estimate the parameters of a non-rigid, free-breathing motion model from a set of projections of thorax that are acquired using a slow rotating CBCT scanner.

RIGID AND DEFORMABLE IMAGE REGISTRATION

Development of an effective image registration technique has been one of the most important research areas. Depending on the mathematical nature of the transformation, image registration is divided into rigid and deformable registrations. In rigid transformations, it is assumed that the geometry of the object is identical in the 2 input images and no distortion occurs in the image acquisition process. A rigid transformation consists of 6 degrees of freedom: 3 displacement parameters and 3 rotational parameters. Deformable registration, on the other hand, is more complicated and entails the modeling of voxel dependent distortion. Clinically, the need for a robust image registration algorithm to compare/fuse images representing the same structures imaged under different conditions or on different modalities is ever increasing because of the extensive use of multi-modality imaging and the emergence of new imaging techniques and methods.

Computer-based rigid image registration has gained widespread popularity in the last decade and is used in routine clinical practice. In this approach, the matching of the 2 input images is formulated into an optimization problem and the best registration of the 2 images is obtained by iteratively comparing various possible matches until no better registration can be found. The search for the optimal match of the 2 input images is usually gauged by a ranking function constructed based on some physical considerations. Depending on the nature of the input images, the formulation of the problem can be highly complicated. Court and Dong[139] used a rigid transformation for the correction of tissue displacement. A deformable procedure based on the finite element model (FEM), in which images are described as blocks of elastic materials on which forces apply, was proposed by Bharath et al.[140] and Brock et al.[141] In this approach, the parameters that control the behavior of the elastic material and are responsible for the conversion of forces into local deformations of the elastic material are

Young's elastic modulus and Poisson's ratio. Although powerful, the model has the drawback that values of the elasticity and density constant for various tissues are not readily available and have to be found by a trial and error procedure. The method also relies on using complicated software to generate a FEM mesh and masks of the involved structures. Schreibmann and Xing have proposed a general narrow-band approach for deformable registration.[93] Depending on the problem, modeling of individual voxel movement can also be made using either B-splines,[79] thinplate splines[142,143,], optical flow algorithms,[144] or fluid flow algorithms.[145] Spline interpolation is a relatively simple approach and our experience with the algorithm suggested that the free-form registration is stable and accurate for dealing with IGRT image registration problems.[146] An improvement to this method can be achieved by using a spline model with the smoothness of the deformation field assured by the interpolation between a grid of fixed control points. A simple method along this line is to deduce the spline coefficients from a set of user-defined control points, as was done by Fei et al.[147] and Lian et al.[143] in warping and registration of MR volumes. Coselmon et al.[148] used a similar technique to study the accuracy of mutual-information-based CT registration of the lung at exhale and inhale respiratory states.

To facilitate the computer decision-making process, image pre-processing or user interaction may be required, especially when dealing with a deformable image registration. The use of homologous anatomic landmark pairs on the 2 input images or the control points is an example of this. In reality, the user must have a detailed understanding of the patient anatomy and the characteristics of the 2 modalities in order to accurately identify the control points on both images. The point pairs are usually obtained interactively with the user repetitively exploring the input image sets and each time trying to locate a point in both of them. Due to the 3D nature, the process is rather tedious and difficult to perform. Schreibmann and Xing[149] have developed a general method to facilitate the selection of control points for both rigid and deformable image registrations. Instead of relying on the interactive selection of homologous control point pairs on both model and reference images, in the proposed approach the user needs only to identify some small control volumes on the model image in a somewhat arbitrary fashion. This new way of image registration eliminates the need for the manual placement of the homologous control points and allows us to register the 2 images accurately and efficiently. The method was applied to both rigid and non-rigid image registration problems and our results indicated that the registration is reliable and provides a valuable tool for intra- or inter-modality image registration. In Fig. 13, we show the registration result of a rectal cancer patient who has undergone both CT and FLT-PET scans. The increased robustness and confidence in the registration and the
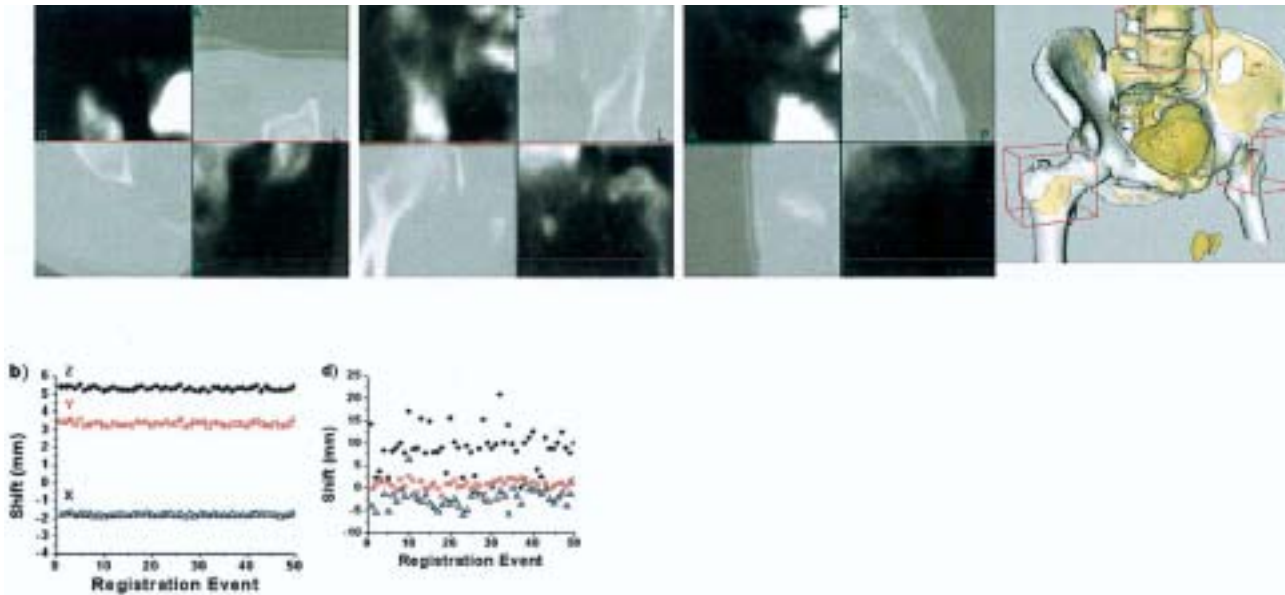
Fig. 13. Sagittal, coronal, and axial views of the CT and FLT-PET registration. In addition to the checkerboard display, a 3D view of the registration is also presented, where an excellent coincidence is observed between the bony structures revealed in CT (white) and PET images (orange). The right 2 panels of the 2nd row show the convergence behaviors of our method and the conventional method for 50 independent calculations. Our method leads to reproducible shifts in x-, y-, and z-directions, and the conventional approach based on the information contained in the whole image entity leads to large variations in the shifts.

increased speed of calculation, especially in the case of the deformable registration, are important features of the new technique. Compared to the manual rigid registration, this method eliminates the nuisance of the control point pair selection and removes a potential source of error in registration. Compared to the automated method, the technique is more intuitive and robust, especially in the presence of image artifacts.

CLINICAL EXPERIENCE WITH IGRT

Clinically implemented IGRT techniques at Stanford include 4D CT, 4D PET, Varian OBI (both planar and CBCT), gating, and Accuray CyberKnife. Several image-guided clinical protocols are under investigation. 4D CT/PET information are used in about 40% of the thorax and upper abdomen cases for patient specific tumor margin definition in 3.5D radiation therapy or for treatment planning of gated radiation therapy. CBCT is mainly applied for patient setup in the treatment of head-and-neck, and prostate and other pelvic diseases. For these sites, the CBCT image quality is reasonable to visualize soft tissues, but the quality is generally notably inferior to that of the state-of-the-art multi-slice fan beam CT scanner. Scan truncation artifacts because the patient shadow does not fit on the detector and/or organ motion often cause Hounsfield unit calibration problems. While this does not seem to influence the image registration, the use of CBCT for dose calculation should proceed with caution. Our initial experience indicates that, when com-

pared with traditional CT-based calculation, the dosimetric error is typically less than 3% for prostate or head-and-neck cases but could be significantly greater in the thoracic region. Comparison between cone beam data and portal image derived setup errors show only slight differences ($<$ 2 mm). However, we should note that the differences are derived purely based on the use of manufacturer-provided image-fusion software, which often emphasizes the high-intensity voxels in bony structures. The next step is to implement soft-tissue based setup corrections clinically. In reality, volumetric data contain much more information compared to planar images, and CBCT promises to be more useful in the future when it is better integrated with treatment planning and delivery systems. An ideal integration would be to use volumetric image-derived information to "tweak" or re-optimize the treatment plan. This work is still in progress at Stanford.

As another example of IGRT treatment, we describe our phase I and II pancreatic tumor dose escalation protocol. The aim is to use CyberKnife to target pancreatic tumors more precisely and to limit the toxicities associated with treatment. In a phase I study, we treated patients with a single fraction of 15, 20, and 25 Gy to unresectable pancreatic tumors using the Cyberknife stereotactic radiotherapy (SRT) system (Accuray).[150] To track tumor movement, we implant fiducial seeds percutaneously into the pancreatic tumor. Using the Accuray Synchrony platform, a model in which the position of the internal fiducials is correlated with the patient's respira-
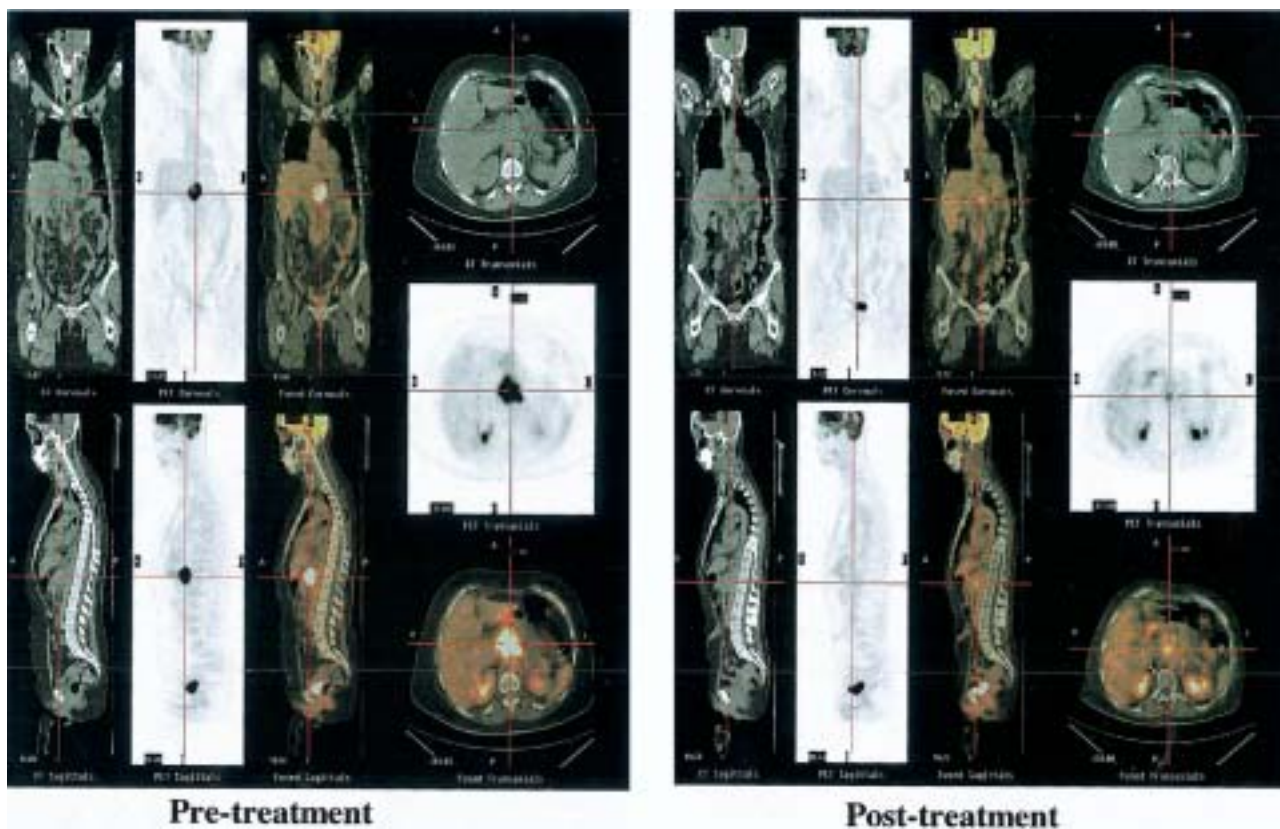
Fig. 14. FDG-PET images of a pancreatic patient before and after radiation therapy.

tory motion is developed. The Cyberknife is able to make real-time corrections to compensate for tumor movement during respiration. Prior to treatment, patients underwent 4D planning CT scans. Using this data set, we are able to visualize how the pancreatic tumor moves/deforms through respiration and compensate for these dynamic changes.[151] Minimal acute gastrointestinal toxicity was observed even at the highest dose. All patients who received 25 Gy had no further local progression of their tumor until death. In a follow up phase II study, a cohort of 19 patients were treated with 45-Gy conventionally fractionated radiation therapy using IMRT to the pancreas and regional lymph nodes followed by a 25-Gy Cyberknife stereotactic radiotherapy boost to the primary tumor.[152] An excellent rate of local control with this therapy was confirmed. Because of the rapid progression of systemic disease, we did not observe a significant improvement in overall survival as compared to historic controls. However, most patients had a clinical benefit (decreased pain, increased activity) and decreased serum tumor marker for pancreatic cancer (CA-19-9) following therapy. To document that SRS truly resulted in an anti-tumor effect, we routinely obtain FDG-PET/CT scans before and after treatment. Figure 14 is an example of one such study. There was intense metabolic activity of the pancreatic tumor prior to therapy with a near complete resolution of FDG uptake in this patient 4

weeks following therapy. The technological challenge for IGRT to minimize toxicity in this clinical scenario is the precision delivery of high-dose radiotherapy. This cannot be accomplished without taking into account the respiratory associated motion of pancreatic tumors. This movement takes place in multiple planes and can result in tumor displacement of up to 1–2 cm. Furthermore, tumor and organ deformation during respiration must also be compensated for during therapy.

SUMMARY

With the development of IMRT during the 1990s, radiation therapy entered a new era. This new process of treatment planning and delivery shows significant potential for improving the therapeutic ratio and offers a valuable tool for dose escalation and/or radiation toxicity reduction. The improved dose conformity and steep dose gradients necessitate enhanced precision and accuracy in patient localization and spawn the development of IGRT, in which various metabolic and anatomical imaging techniques are integrated into the radiation therapy process. The overall goal of IGRT is to target tumors more accurately while better sparing the normal tissues. Much recent effort is focused on removing the uncertainty in the definition of the target volume and in the determination of the position of mobile and often deformable

organs. Biological imaging described in this article will allow us not only to delineate the boundary of the tumor volume based on the tumors' biological characteristics but also to map out the biology distribution of the cancer cells, affording a significant opportunity for BCRT treatment in the future. Developments of effective 4D CT/PET techniques will provide effective means for us to understand the temporal dependence of the involved structures and design the best possible strategy for targeting the moving tumor. Integration of various imaging tools for off-line and on-line application is also of paramount importance, enabling us to ensure the planned dose distributions can be realized in the clinical setting. With the newly available IGRT tools, physicians will be able to optimize radiotherapy accuracy and precision by adjusting the radiation beam based on the actual positions of the target tumor and critical organs during radiation therapy planning and treatment. We should mentioned that IGRT is still in its infancy and many technical issues remain to be resolved, such as the establishment of a robust deformable registration method, auto-mapping of the contours outlined on the planning CT to CBCT or to different phases of 4D CT, and management of the sheer volume of acquired image sets (both 4D CT/PET and CBCT). However, it is believed that much of these technical hurdles will be resolved with time, and that IGRT will become the standard of practice in the future through the effort of researchers around the world.

REFERENCES

1. IMRT Collaborative Working Group: Intensity-modulated radiotherapy: Current status and issues of interest. *Int. J. Radiat. Oncol. Biol. Phys.* **51**:880–914; 2001.
2. AAPM IMRT Sub-Committee: Guidance document on delivery, treatment planning, and clinical implementation of IMRT: Report of the IMRT Subcommittee of the AAPM Radiation Therapy Committee. *Med. Phys.* **30**:2089–115; 2003.
3. Galvin, J.M.; Ezzell, G.; Eisbrauch, A.; *et al.* Implementing IMRT in clinical practice: A joint document of the American Society for Therapeutic Radiology and Oncology and the American Association of Physicists in Medicine. *Int. J. Radiat. Oncol. Biol. Phys.* **58**:1616–34; 2004.
4. Hamilton, R.J.; Sweeney, P.J.; Pelizzari, C.A.; *et al.* Functional imaging in treatment planning of brain lesions. *Int. J. Radiat. Oncol. Biol. Phys.* **37**:181–8; 1997.
5. Sawada, A.; Yoda, K.; Kokubo, M.; *et al.* A technique for noninvasive respiratory gated radiation treatment system based on a real time 3D ultrasound image correlation: A phantom study. *Med. Phys.* **31**:245–50; 2004.
6. Yu, Y.; Anderson, L.L.; Li, Z.; *et al.* Permanent prostate seed implant brachytherapy: Report of the American Association of Physicists in Medicine Task Group No. 64. *Med. Phys.* **26**:2054–76; 1999.
7. Pirzkall, A.; McKnight, T.R.; Graves, E.E.; *et al.* MR-spectroscopy guided target delineation for high-grade gliomas. *Int. J. Radiat. Oncol. Biol. Phys.* **50**:915–28; 2001.
8. Kurhanewicz, J.; Hricak, H.; Sokolov, D.L.; *et al.* Prostate cancer: Localization with three-dimensional proton MR spectroscopic imaging—clinicopathologic study. *Radiology* **206**:785–90; 1998.
9. DiBiase, S.J.; Hosseinzadeh, K.; Gullapalli, R.P.; *et al.* Magnetic resonance spectroscopic imaging-guided brachytherapy for localized prostate cancer. *Int. J. Radiat. Oncol. Biol. Phys.* **52**:429–38; 2002.
10. Kim, D.H.; Margolis, D.; Xing, L.; *et al.* In vivo prostate magnetic resonance spectroscopic imaging using two-dimensional J-resolved PRESS at 3 T. *Magn. Reson. Med.* **53**:1177–82; 2005.
11. Zaider, M.; Zelefsky, M.J.; Lee, E.K.; *et al.* Treatment planning for prostate implants using magnetic-resonance spectroscopy imaging. *Int. J. Radiat. Oncol. Biol. Phys.* **47**:1085–96; 2000.
12. Hunjan, S.; Gibbs, I.; Spielman, D.M.; *et al.* Validating magnetic resonance spectroscopic imaging for radiation therapy guidance. *Int. J. Radiat. Oncol. Biol. Phys.* **57**:1159–73; 2003.
13. Townsend, D.W.; Carney, J.P.; Yap, J.T.; *et al.* PET/CT doday and tomorrow. *J. Nucl. Med.* **45**:4S–14S; 2004.
14. Czernin, J.; Schelbert, H. PET/CT imaging, facts, options, hopes, and questions. *J. Nucl. Med.* **45**:1S–3S; 2004.
15. Hicks, R.J.; Kalff, V.; MacManus, M.P.; *et al.* (18)F-FDG PET provides high-impact and powerful prognostic stratification in staging newly diagnosed non-small cell lung cancer. *J. Nucl. Med.* **42**:1596–604; 2001.
16. Mac Manus, M.P.; Hicks, R.J.; Ball, D.L.; *et al.* F-18 fluorodeoxyglucose positron emission tomography staging in radical radiotherapy candidates with nonsmall cell lung carcinoma: Powerful correlation with survival and high impact on treatment. *Cancer* **92**:886–95; 2001.
17. Bradley, J.D.; Dehdashti, F.; Mintun, M.A.; *et al.* Positron emission tomography in limited-stage small-cell lung cancer: A prospective study. *J. Clin. Oncol.* **22**:3248–54; 2004.
18. Howard, A.; Mehta, M.P.; Ritter, M.A.; *et al.* The value of PET/CT in gross tumor volume delineation in lung and esophagus cancer. *Int. J. Radiat. Oncol. Biol. Phys.* **60**:S536–537; 2004.
19. Hofer, C.; Laubenbacher, C.; Block, T.; *et al.* Fluorine-18-fluorodeoxyglucose PET is useless for the detection of local recurrence after radical prostatectomy. *Eur. Urol.* **36**:31–5; 1999.
20. Liu, I.J.; Zafar, M.B.; Lai, Y.H.; *et al.* Fluorodeoxyglucose PET studies in diagnosis and staging of clinically organ-confined prostate cancer. *Urology* **57**:108–11; 2001.
21. Gambhir, S.S.; Srinivasan, A.; Banerjee, P.K.; *et al.* PET in oncology: Will it replace the other modalities? *J. Nucl. Med.* **39**:729–34; 1998.
22. Gambhir, S.S. Molecular imaging of cancer with PET. *Nat. Rev. Cancer* **2**:683–93; 2002.
23. Schèoder, H.; Larson, S.M. Positron emission tomography for prostate, bladder, and renal cancer. *Semin. Nucl. Med.* **34**:274–92; 2004.
24. Buck, A.K.; Halter, G.; Schirrmeister, H.; *et al.* Imaging proliferation in lung tumors with PET: 18F-FLT versus 18F-FDG. *J. Nucl. Med.* **44**:1426–31; 2003.
25. Shields, A.F.; Grierson, J.R.; Dohmen, B.M.; *et al.* Imaging proliferation in vivo with [F-18]FLT and positron emission tomography. *Nat. Med.* **4**:1334–6; 1998.
26. Buck, A.K.; Schirrmeister, H.; Hetzel, M.; *et al.* 3-deoxy-3-[(18)F]fluorothymidine-PET for noninvasive assessment of proliferation in pulmonary nodules. *Cancer Res.* **62**:3331–4; 2002.
27. Smyczek-Gargya, B.; Fersis, N.; Dittmann, H.; *et al.* PET with [18F]fluorothymidine for imaging of primary breast cancer: A pilot study. *Eur. J. Nucl. Med. Mol. Imag.* **31**:720–724.
28. Shreve, P.D.; Gross, M.D. Imaging of the pancreas and related diseases with PET carbon-11-acetate. *J. Nucl. Med.* **38**:1305–10; 1997.

29. Seltzer, M.A.; Jahan, S.A.; Sparks, R.; *et al.* Radiation dose estimates in humans for (11)C-acetate whole-body PET. *J. Nucl. Med.* **45:**1233–6; 2004.

30. Jager, P.L.; Que, T.H.; Vaalburg, W.; *et al.* Carbon-11 choline or FDG-PET for staging of oesophageal cancer? *Eur. J. Nucl. Med.* **28:**1845–9; 2001.

31. Ishiwata, K.; Kasahara, C.; Hatano, K.; *et al.* Carbon-11 labeled ethionine and propionine as tumor detecting agents. *Ann. Nucl. Med.* **1:**115–22; 1997.

32. Iozzo, P.; Osman, S.; Glaser, M.; *et al.* In vivo imaging of insulin receptors by PET: Preclinical evaluation of iodine-125 and iodine-124 labelled human insulin. *Nucl. Med. Biol.* **29:**73–82; 2002.

33. Herlin, G.; Persson, B.; Bergstrèom, M.; *et al.* 11C-harmine as a potential PET tracer for ductal pancreas cancer: In vitro studies. *Eur Radiol.* **13:**729–3; 2003.

34. Brown, W.D.; Oakes, T.R.; DeJesus, O.T.; *et al.* Fluorine-18-fluoro-L-DOPA dosimetry with carbidopa pretreatment. *J. Nucl. Med.* **39:**1884–91; 1998.

35. Blankenberg, F.G.; Strauss, H.W. Nuclear medicine applications in molecular imaging. *J. Magn. Res. Imaging* **16:**352–61; 2002.

36. Oyama, N.; Akino, H.; Kanamaru, H.; *et al.* 11C-acetate PET imaging of prostate cancer. *J. Nucl. Med.* **43:**181–6; 2002.

37. Kotzerke, J.; Volkmer, B.G.; Glatting, G.; *et al.* Intraindividual comparison of [11C]acetate and [11C]choline PET for detection of metastases of prostate cancer. *Nuklearmedizin* **42:**25–30; 2003.

38. Mathews, D.; Oz, O.K. PET in prostate and renal cell carcinoma. *Curr. Opin. Urol.* **12:**381–5; 2002.

39. DeGrado, T.R.; Baldwin, S.W.; Wang, S.; *et al.* Synthesis and evaluation of (18)F-labeled choline analogs as oncologic PET tracers. *J. Nucl. Med.* **42:**1805–14; 2001.

40. Hara, T.; Kosaka, N.; Kishi, H. Development of (18)F-fluoroethylcholine for cancer imaging with PET: Synthesis, biochemistry, and prostate cancer imaging. *J. Nucl. Med.* **43:**187–99; 2002.

41. Hara, T.; Kosaka, N.; Kishi, H. PET imaging of prostate cancer using carbon-11-choline. *J. Nucl. Med.* **39:**990–5; 1998.

42. Sutinen, E.; Nurmi M.; Roivainen A.; *et al.* Kinetics of [(11)C]choline uptake in prostate cancer: A PET study. *Eur. J. Nucl. Med. Mol. Imaging* **31:**317–24; 2004.

43. Chen, X.; Park, R.; Hou, Y.; *et al.* MicroPET and autoradiographic imaging of GRP receptor expression with 64Cu-DOTA-[Lys3]bombesin in human prostate adenocarcinoma xenografts. *J. Nucl. Med.* **45:**1390–7; 2004.

44. Rasey, J.S.; Koh, W.J.; Evans, M.L.; *et al.* Quantifying regional hypoxia in human tumors with positron emission tomography of [18F]fluoromisonidazole: A pretherapy study of 37 patients. *Int. J. Radiat. Oncol. Biol. Phys.* **36:**417–28; 1996.

45. O'Donoghue, J.A.; Zanzonico, P.; Pugachev, A.; *et al.* Assessment of regional tumor hypoxia using 18F-fluoromisonidazole and 64Cu(II)-diacetyl-bis(N4-methylthiosemicarbazone) positron emission tomography: Comparative study featuring microPET imaging, Po2 probe measurement, autoradiography, and fluorescent microscopy in the R3327-AT and FaDu rat tumor models. *Int. J. Radiat. Oncol. Biol. Phys.* **61:**1493–502; 2005.

46. Piert, M.; Machulla, H.J.; Picchio, M.; *et al.* Hypoxia-specific tumor imaging with 18F-fluoroazomycin arabinoside. *J. Nucl. Med.* **46:**106–13; 2005.

47. Chao, K.S.; Mutic, S.; Gerber, R.L.; *et al.* A novel approach to overcome hypoxic tumor resistance: Cu-ATSM-guided intensity-modulated radiation therapy. *Int. J. Radiat. Oncol. Biol. Phys.* **49:**1171–82; 2001.

48. de Jong I.J.; Pruim, J.; Elsinga, P.H.*; et al.* 11C-choline positron emission tomography for the evaluation after treatment of localized prostate cancer. *Eur. Urol.* **44:**327–8; discussion 38–9; 2003.

49. Ling, C.C.; Humm, J.; Larson, S.; *et al.* Towards multidimensional radiotherapy (MD-CRT): Biological imaging and biological conformality. *Int. J. Radiat. Oncol. Biol. Phys.* **47:**551–60; 2000.

50. Brahme, A. Individualizing cancer treatment: Biological optimization models in treatment planning and delivery. *Int. J. Radiat. Oncol. Biol. Phys.* **49:**327–37; 2001.

51. Xing, L.; Cotrutz, C.; Hunjan, S.; *et al.* Inverse planning for functional image-guided IMRT. *Phys. Med. Biol.* **47:**3567–78; 2002.

52. Alber, M.; Paulsen, F.; Eschman, S.M.; *et al.* On biologically conformal boost dose optimization. *Phys. Med. Biol.* **48:**N31–5; 2003.

53. Yang, Y.; Xing, L. Towards biologically conformal radiation therapy (BCRT): Selective IMRT dose escalation under the guidance of spatial biology distribution. *Med. Phys.* **32:**1473–84; 2005.

54. Seppenwoolde, Y.; Shirato, H.; Kitamura, K.; *et al.* Precise and real-time measurement of 3D tumor motion in lung due to breathing and heartbeat, measured during radiotherapy. *Int. J. Radiat. Oncol. Biol. Phys.* **53:**822; 2002.

55. Shirato, H.; Seppenwoolde, Y.; Kitamura, K.; *et al.* Intrafractional tumor motion: Lung and liver. *Semin. Radiat. Oncol.* **14:**10–8; 2004.

56. Shimizu, S.; Shirato, H.; Ogura, S.; *et al.* Detection of lung tumor movement in real-time tumor-tracking radiotherapy. *Int. J. Radiat. Oncol. Biol. Phys.* **51:**304–10; 2001.

57. Xu, Q.; Hamilton, R. Novel respiratory gating method based on automated analysis of ultrasonic diaphragm motion. *Med. Phys.* **32:**2124; 2005.

58. Huang, M.H.; Lin, Y.S.; Lee, C.L.; *et al.* Use of ultrasound to increase effectiveness of isokinetic exercise for knee osteoarthritis. *Arch. Phys. Med. Rehabil.* **86:**1545–51; 2005.

59. Seiler, P.G.; Blattmann, H.; Kirsch S.; *et al.* A novel tracking technique for the continuous precise measurement of tumour positions in conformal radiotherapy. *Phys. Med. Biol.* **45:**N103–10; 2000.

60. Balter, J.M.; Wright, J.N.; Newell, L.J.; *et al.* Accuracy of a wireless localization system for radiotherapy. *Int. J. Radiat. Oncol. Biol. Phys.* **61:**933–7; 2005.

61. Nehmeh, S.A.; Erdi, Y.E.; Pan, T.; *et al.* Four-dimensional (4D) PET/CT imaging of the thorax. *Med. Phys.* **31:**3179; 2004.

62. Thorndyke, B.; Schreibmann, E.; Maxim, P.; et al. Enhancing 4D PET through retrospective stacking. Presented at 2005 Annual Meeting of American Association of Physicists in Medicine, Seattle, WA, 2005.

63. Thorndyke, B.; Schreibmann, E.; Xing, L. Reducing motion artifacts in PET through retrospective stacking. Med. Phys. **33:**2006; In press.

64. Vedam, S.S.; Keall, P.J.; Kini, V.R.; *et al.* Acquiring a four-dimensional computed tomography dataset using an external respiratory signal. *Phys. Med. Biol.* **48:**45; 2003.

65. Keall, P.J.; Starkschall, G.; Shukla, H.; *et al.* Acquiring 4D thoracic CT scans using a multislice helical method. *Phys. Med. Biol.* **49:**2053–67; 2004.

66. Low. D.A.; Nystrom, M.; Kalinin, E.; *et al.* A method for the reconstruction of four-dimensional synchronized CT scans acquired during free breathing. *Med. Phys.*

67. Rietzel, E.; Pan, T.; Chen, G.T.Y. Four-dimensional computed tomography: Image formation and clinical protocol. *Med. Phys.* **32:**874; 2005.

68. Li, T.; schreibmann, E.; Thorndyke, B.; *et al.* Radiation dose reduction in 4D CT. Med. Phys. In press.

69. Kubo, H.D.; Len, P.M.; Minohara, S.; *et al.* Breathing-synchronized radiotherapy program at the University of California Davis Cancer Center. *Med. Phys.* **27:**346; 2000.

70. Rueckert, D.; Sonoda, L.I.; Hayes, C.; *et al.* Nonrigid registration using free-form deformations: Application to breast MR images. *IEEE Trans. Med. Imaging* **18:**712–21; 1999.

71. Pan, T.; Lee, T.-Y.; Rietzel, E.; *et al.* 4D-CT imaging of a volume influenced by respiratory motion on multi-slice CT. *Med. Phys.* **31:**333; 2004.

72. Kini, V.R.; Vedam, S.S.; Keall, P.J.; *et al.* Patient training in respiratory-gated radiotherapy. *Med. Dosim.* **28:**7; 2003.

73. Wong, J.W.. Sharpe, M.B.; Jaffray, D.A.*; et al.* The use of active breathing control (ABC) to reduce margin for breathing motion. *Int. J. Radiat. Oncol. Biol. Phys.* **44:**911; 1999.

74. Frazier, R.C.; Vicini, F.A.; Sharpe, M.B.; *et al.* Impact of breathing motion on whole breast radiotherapy: A dosimetric analysis using active breathing control. *Int. J. Radiat. Oncol. Biol. Phys.* **58:**1041–7; 2004.

75. Dawson, L.A.; Brock, K.K.; Kazanjian, S.; *et al.* The reproducibility of organ position using active breathing control (ABC) during liver radiotherapy. *Int. J. Radiat. Oncol. Biol. Phys.* **51:**1410–21; 2001.

76. Starkschall, G.; Himanshu, S.; Keall, P.J.; et al. Displacement-based binning of 4-D CT image data sets. XIVth International Conference on the Use of Computers in Radiation Therapy, 2004, pp 53.

77. Thorndyke, B.; Schreibmann, E.; Li, T.; *et al.* A comparison of amplitude- and phase-based 4D CT. *Med. Phys.* **32:**1919; 2005.

78. Lu, W.; Parikh, P.; Bradley, J.; *et al.* A comparison between amplitude sorting and phase sorting using external respiratory measurements for 4D CT. *Med. Phys.* **32:**2094; 2005.

79. Schreibmann, E.; Chen, G.T.Y.; Xing, L. Image interpolation in 4D CT using a BSpline deformable registration model. *Int. J. Radiat. Oncol. Biol. Phys.* 2006; In press.

80. Schweikard, A.; Shiomi, H.; Fisseler, J.; et al. Fiducial-less respiration tracking in radiosurgery. LNCS **3217:**992–99; 2004.

81. Vedam, S.S.; Kini, V.R.; Keall, P.J.; *et al.* Quantifying the predictability of diaphragm motion during respiration with a noninvasive external marker. *Med. Phys.* **30:**505; 2003.

82. Ford, E.C.; Mageras, G.S.; Yorke, E.; *et al.* Evaluation of respiratory movement during gated radiotherapy using film and electronic portal imaging. *Int. J. Radiat. Oncol. Biol. Phys.* **52:**522; 2002.

83. Yorke, E.; Rosenzweig, K.E.; Wagman, R.; *et al.* Interfractional anatomic variation in patients treated with respiration-gated radiotherapy. *J. Appl. Clin. Med. Phys.* **6:**19; 2005.

84. Klein, G.J.; Reutter, B.W.; Ho, M.H.; *et al.* Real-time system for respiratory-cardiac gating in positron tomography. *IEEE Trans. Nucl. Sci.* **45:**2139; 1998.

85. Nehmeh, S.A.; Erdi, Y.E.; Ling, C.C.; *et al.* Effect of respiratory gating on quantifying PET images of lung cancer. *J. Nucl. Med.* **43:**876–81; 2002.

86. Nehmeh, S.A.; Erdi, Y.E.; Rosenzweig, K.E.; *et al.* Reduction of respiratory motion artifacts in PET imaging of lung cancer by respiratory correlated dynamic PET: Methodology and comparison with respiratory gated PET. *J. Nucl. Med.* **44:**1644; 2003.

87. Cherry, S.R.; Dahlborn, M. Physics, Instrumentation and Scanners, PET: Molecular Imaging and its Biological Applications. New York: Springer-Verlag; 2004.

88. Sarikaya, I.; Yeung, H.W.; Erdi, Y.; *et al.* Respiratory artefact causing malpositioning of liver dome lesion in right lower lung. *Clin. Nucl. Med.* **28:**943; 2003.

89. Erdi, Y.E.; Nehmeh, S.A.; Pan, T.; *et al.* The CT motion quantitation of lung lesions and its impact on PET-measured SUVs. *J. Nucl. Med.* **45:**1287; 2004.

90. Pevsner, A.; Nehmeh, S.A.; Humm, J.L.; *et al.* Effect of motion on tracer activity determination in CT attenuation corrected PET images: A lung phantom study. *Med. Phys.* **32:**2358; 2005.

91. Nehmeh, S.A.; Erdi, Y.E.; Pan, T.; *et al.* Quantitation of respiratory motion during 4D-PET/CT acquisition. *Med. Phys.* **31:** 1333–8; 2004.

92. Mattes, D.; Haynor, R.D.; Vesselle, H.; *et al.* PET-CT image registration in the chest using free-form deformations. *IEEE Trans. Med. Imaging* **22:**120–28; 2003.

93. Schreibmann, E.; Xing, L. Narrow band deformable registration of prostate MRI/MRSI and CT studies. *Int. J. Radiat. Oncol. Biol. Phys.* **62:**595–605; 2005.

94. Li, T.; Thorndyke, B.; Schreibmann, E.; et al. Model-based image reconstruction for four-dimensional PET. Med. Phys. Submitted.

95. Trofimov, A.; Rietzel, E.; Lu, H.M.; *et al.* Temporo-spatial IMRT optimization: Concepts, implementation and initial results. *Phys. Med. Biol.* **50:**2779–98; 2005.

96. Armbruster, B.; Yang, Y.; Schreibmann, E.; et al. Inverse planning for time-resolved aperture modulated radiation therapy. Annual ASTRO Meeting, Denver, CO, 2005.

97. Bortfeld, T.; Jiang, S.B.; Rietzel, E. Effects of motion on the total dose distribution. *Semin. Radiat. Oncol.* **14:**41–51; 2004.

98. Jiang, S.B.; Pope, C.; Al Jarrah, K.M.*; et al.* An experimental investigation on intra-fractional organ motion effects in lung IMRT treatments. *Phys. Med. Biol.* **48**:1773–84; 2003.

99. Rietzel, E.; Chen, G.T.; Choi, N.C.; *et al.* 4D image-based treatment planning: Target volume segmentation and dose calculation in the presence of respiratory motion. *Int. J. Radiat. Oncol. Biol. Phys.* **61:**1535; 2005.

100. Keall, P.J.; Joshi, S.; Vedam, S.S.; *et al.* Four-dimensional radiotherapy planning for DMLC-based respiratory motion tracking. *Med. Phys.* **32:**942–51; 2005.

101. Webb, S. The effect on IMRT conformality of elastic tissue movement and a practical suggestion for movement compensation via the modified dynamic multileaf collimator technique. *Phys. Med. Biol.* **50:**1163–90; 2005.

102. Yang, Y.; Xing, L. Clinical knowledge-based inverse treatment planning. *Phys. Med. Biol.* **49:**5101–17; 2004.

103. Yang, Y.; Xing, L. Inverse treatment planning with adaptively evolving voxel-dependent penalty scheme. *Med. Phys.* **31:**2839–44; 2004.

104. Wu, Q.; Mohan, R.; Niemierko, A.; *et al.* Optimization of intensity-modulated radiotherapy plans based on the equivalent uniform dose. *Int. J. Radiat. Oncol. Biol. Phys.* **52:**224–35; 2002.

105. Olivera, G.H.; Shepard, D.M.; Reckwerdt, P.J.; *et al.* Maximum likelihood as a common computational framework in tomotherapy. *Phys. Med. Biol.* **43:**3277–94; 1998.

106. Lee, E.K.; Gallagher, R.J.; Silvern, D.; *et al.* Treatment planning for brachytherapy: An integer programming model, two computational approaches and experiments with permanent prostate implant planning. *Phys. Med. Biol.* **44:**145–65; 1999.

107. Shepard, D.M.; Earl, M.A.; Li, X.A.; *et al.* Direct aperture optimization: A turnkey solution for step-and-shoot IMRT. *Med. Phys.* **29:**1007–18; 2002.

108. Bednarz, G.; Michalski, D.; Houser, C.; *et al.* The use of mixed-integer programming for inverse treatment planning with predefined field segments. *Phys. Med. Biol.* **47:**2235–45; 2002.

109. Cotrutz, C.; Xing, L. Segment-based dose optimization using a genetic algorithm. *Phys. Med. Biol.* **48:**2987–98; 2003.

110. Murphy, M.J.; Adler, Jr.; J.R Bodduluri, M.*; et al.* Image-guided radiosurgery for the spine and pancreas. *Comput. Aided Surg.* **5:**278–88; 2000.

111. Murphy, M.J. Tracking moving organs in real time. *Semin. Radiat. Oncol.* **14:**91–100; 2004.

112. Sharp, G.C.; Jiang, S.B.; Shimizu, S.; *et al.* Prediction of respiratory tumour motion for real-time image-guided radiotherapy. *Phys. Med. Biol.* **49:**425–40; 2004.

113. Berbeco, R.I.; Neicu, T.; Rietzel, E.; *et al.* A technique for respiratory-gated radiotherapy treatment verification with an EPID in cine mode. *Phys. Med. Biol.* **50:**3669–79; 2005.

114. Herman, M.G.; Balter, J.M.; Jaffray, D.A.;*et al.* Clinical use of electronic portal imaging: Report of AAPM Radiation Therapy Committee Task Group 58. *Med. Phys.* **28:**712–37; 2001.

115. Yang, Y.; Xing, L. Quantitative measurement of MLC leaf displacements using an electronic portal image device. *Phys. Med. Biol.* **49:**1521–33; 2004.

116. Yan, D.; Wong, J.; Vicini, F.; *et al.* Adaptive modification of treatment planning to minimize the deleterious effects of treatment setup errors. *Int. J. Radiat. Oncol. Biol. Phys.* **38:**197–206; 1997.

117. Court, L.E.; Dong, L.; Taylor, N.; *et al.* Evaluation of a contour-alignment technique for CT-guided prostate radiotherapy: An intra- and interobserver study. *Int. J. Radiat. Oncol. Biol. Phys.* **59:**412–8; 2004.

118. Orton, N.P.; Tome, W.A. The impact of daily shifts on prostate IMRT dose distributions. *Med. Phys.* **31:**2845–8; 2004.

119. Fuss, M.; Salter, B.J.; Cavanaugh, S.X.; *et al.* Daily ultrasound-based image-guided targeting for radiotherapy of upper abdominal malignancies. *Int. J. Radiat. Oncol. Biol. Phys.* **59:**1245–56; 2004.

120. Saw, C.B.; Ayyangar, K.M.; Zhen, W.; *et al.* Clinical implementation of intensity-modulated radiation therapy. *Med. Dosim.* **27:** 161–9; 2002.

121. Schweikard, A.; Glosser, G.; Bodduluri, M.; *et al.* Robotic motion compensation for respiratory movement during radiosurgery. *Comput. Aided Surg.* **5:**263–77; 2000.

122. Mackie, T.R.; Balog, J.; Ruchala, K.; *et al.* Tomotherapy. *Semin. Radiat. Oncol.* **9:**108–17; 1999.

123. Meeks, S.; Harmon, J.J.; Langen, K.; *et al.* Performance characterization of megavoltage computed tomography imaging on a helical tomotherapy unit. *Med. Phys.* **32:**2673–81; 2005.

124. Jaffray, D.A.; Siewerdsen, J.H.; Wong, J.W.; *et al.* Flat-panel cone-beam computed tomography for image-guided radiation therapy. *Int. J. Radiat. Oncol. Biol. Phys.* **53:**1337–49; 2002.

125. Pouliot, J.; Bani-Hashemi, A.; Chen, J.; *et al.* Low-dose megavoltage cone-beam CT for radiation therapy. *Int. J. Radiat. Oncol. Biol. Phys.* **61:**552–60; 2005.

126. Oldham, M.; Letourneau, D.; Watt, L.; et al. Cone-beam-CT guided radiation therapy: A model for on-line application. Radiother. Oncol. **75:**271–8; 2005.

127. Li, T.; Yang, Y.; Schreibmann, E.; et al. A new cone-beam CT reposition technique through deformable registration. Annual Meeting of American Association of Physicists in Medicine, Seattle, WA, 2005.

128. Mohan, R.; Zhang, X.; Wang, H.; *et al.* Use of deformed intensity distributions for on-line modification of image-guided IMRT to account for interfractional anatomic changes. *Int. J. Radiat. Oncol. Biol. Phys.* **61:**1258–66; 2005.

129. Yang, Y.; Li, T.; Schreibmann, E.; et al. Is cone beam CT suitable for dose verification? Annual Meeting of American Association of Physicists in Medicine, Seattle, WA, 2005.

130. Yang, Y.; Schreibmann, E.; Xing, L.; et al. Dosimetric evaluation of kV cone-beam CT (CBCT)-based dose calculation. *Phys. Med. Biol.* 2006; Submitted.

131. Wang, G.; Vannier, M.W. Preliminary study on helical CT algorithms for patient motion estimation and compensation. *IEEE Trans. Med. Imaging* **14:**205–11; 1995.

132. Willis, N.P.; Bresler, Y. Optimal scan for time-varying tomography. I: Theoretical analysis and fundamental limitations*IEEE Trans. Med. Imaging* **14:**642–53; 1995.

133. Atalar, E.; Onural, L. A respiratory motion artifact reduction method in magnetic resonance imaging of the chest. *IEEE Trans. Med. Imaging* **10:**11–24; 1991.

134. Crawford, C.; King, K.F.; Ritchie, C.J.; *et al.* Respiratory compensation in projection imaging using a magnification and displacement model. *IEEE Trans. Med. Imaging* **15:**327–32; 1996.

135. Li, T.; Schreibmann, E.; Yang, Y.; Xing, L. Respiratory motion correction with deformation field for improved on-board imaging with cone-beam CT. *Phys. Med. Biol.* **51:**253–67; 2006.

136. Sonke, J.J.; Zijp, L.; Remeijer, P.; *et al.* Respiratory correlated cone beam CT. *Med. Phys.* **32:**1176–86; 2005.

137. Li, T.; Xing, L.; Munro, P.; et al. 4D cone beam CT using an on-board imager. *Med. Phys.* 2006; Submitted.

138. Zeng, R.; Fessler, J.A.; Balter, J.M. Respiratory motion estimation from slowly rotating x-ray projections: Theory and simulation. *Med.Phys.* **32:**984–91; 2005.

139. Court, L.E.; Dong, L. Automatic registration of the prostate for computed-tomography-guided radiotherapy. *Med. Phys.* **30:**2750–7; 2003.

140. Bharath, A.; Hirose, M.; Hata, N.; *et al.* Evaluation of three-dimensional finite element-based deformable registration of pre- and intraoperative prostate imaging. *Med. Phys.* **28:**2551–60; 2001.

141. Brock, K.K.; McShan, D.L.; Balter, J.M. A comparison of computer-controlled versus manual on-line patient setup adjustment. *J. Appl. Clin. Med. Phys.* **3:**241–7; 2002.

142. Bookstein, F.L. Thin plate splines and the decomposition of deformations. *IEEE Trans. Pattern Anal. Mach. Intell.* **11:**567–85; 1989.

143. Lian, J.; Xing, L.; Hunjan, S.; *et al.* Mapping of the prostate in endorectal coil-based MRI/MRSI and CT: A deformable registration and validation study. *Med. Phys.* **31:**3087–94; 2004.

144. Guerrero, T.; Zhang, G.; Huang, T.C.; *et al.* Intrathoracic tumour motion estimation from CT imaging using the 3D optical flow method. *Phys. Med. Biol.* **49:**4147–61; 2004.

145. Mageras, G.S.; Pevsner, A.; Yorke, E.D.; *et al.* Measurement of lung tumor motion using respiration-correlated CT. *Int. J. Radiat. Oncol. Biol. Phys.* **60:**933–41; 2004.

146. Schwartz, D.L.; Ford, E.C.; Rajendran, J.; *et al.* FDG-PET/CT-guided intensity modulated head and neck radiotherapy: A pilot investigation. *Head Neck* **27:**478–87; 2005.

147. Fei, B.; Wheaton, A.; Lee, Z.; *et al.* Automatic MR volume registration and its evaluation for the pelvis and prostate. *Phys. Med. Biol.* **2002:**823–38; 2002.

148. Coselmon, M.M.; Balter, J.M.; McShan, D.L.; *et al.* Mutual information based CT registration of the lung at exhale and inhale breathing states using thin-plate splines. *Med. Phys.* **31:**2942–8; 2004.

149. Schreibmann, E.; Xing, L. Image registration with auto-mapped control volumes. *Med. Phys.* Submitted.

150. Koong, A.C.; Le, Q.T.; Ho, A.; *et al.* Phase I study of stereotactic radiosurgery in patients with locally advanced pancreatic cancer. *Int. J. Radiat. Oncol. Biol. Phys.* **58:**1017–21; 2004.

151. Loo, B.; Thorndyke, B.; Maxim, P.; et al. Determining margin for target deformation and rotation in respiratory motion-tracked stereotactic radiosurgery of pancreatic cancer, Annual ASTRO Meeting, Denver, CO, 2005.

152. Koong, A.C.; Le, Q.T.; Ho, A.; et al. Phase II study of stereotactic radiosurgery in patients with locally advanced pancreatic cancer. *Int. J. Radiat. Oncol. Biol. Phys.* In press.